

New chronological constraints on intense Holocene eruptions and landslide activity at Tacaná volcanic complex (Mexico)

Jesús Alcalá-Reygosa, José Luis Arce, José Luis Macías, Irene Schimmelpfennig, Ricardo Saucedo, Juan Manuel Sánchez, Teodoro Carlón, Rosario Vázquez, Guillermo Cisneros-Máximo, Adrian Jímenez, et al.

▶ **To cite this version:**

Jesús Alcalá-Reygosa, José Luis Arce, José Luis Macías, Irene Schimmelpfennig, Ricardo Saucedo, et al.. New chronological constraints on intense Holocene eruptions and landslide activity at Tacaná volcanic complex (Mexico). Quaternary Geochronology, 2021, 65, pp.101183. 10.1016/j.quageo.2021.101183 . hal-03226096

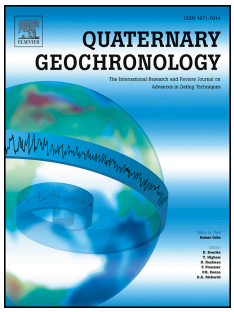
HAL Id: hal-03226096
https://hal.science/hal-03226096

Submitted on 14 May 2021

HAL is a multi-disciplinary open access archive for the deposit and dissemination of scientific research documents, whether they are published or not. The documents may come from teaching and research institutions in France or abroad, or from public or private research centers.

L'archive ouverte pluridisciplinaire **HAL**, est destinée au dépôt et à la diffusion de documents scientifiques de niveau recherche, publiés ou non, émanant des établissements d'enseignement et de recherche français ou étrangers, des laboratoires publics ou privés.

Journal Pre-proof



New chronological constraints on intense Holocene eruptions and landslide activity at Tacana volcanic complex (Mexico)

Jesús Alcalá-Reygosa, José Luis Arce, José Luis Macías, Irene Schimmelpfennig, Ricardo Saucedo, Juan Manuel Sánchez, Teodoro Carlón, Rosario Vázquez, Guillermo Cisneros-Máximo, Adrian Jímenez, Salvador Fernández, Aster Team

PII: S1871-1014(21)00034-0

DOI: https://doi.org/10.1016/j.quageo.2021.101183

Reference: QUAGEO 101183

To appear in: *Quaternary Geochronology*

Received Date: 8 June 2020

Revised Date: 10 April 2021

Accepted Date: 11 April 2021

Please cite this article as: Alcalá-Reygosa, Jesú., Arce, José.Luis., Macías, José.Luis., Schimmelpfennig, I., Saucedo, R., Sánchez, J.M., Carlón, T., Vázquez, R., Cisneros-Máximo, G., Jímenez, A., Fernández, S., Team, A., New chronological constraints on intense Holocene eruptions and landslide activity at Tacana volcanic complex (Mexico), *Quaternary Geochronology* (2021), doi: https://doi.org/10.1016/j.quageo.2021.101183.

This is a PDF file of an article that has undergone enhancements after acceptance, such as the addition of a cover page and metadata, and formatting for readability, but it is not yet the definitive version of record. This version will undergo additional copyediting, typesetting and review before it is published in its final form, but we are providing this version to give early visibility of the article. Please note that, during the production process, errors may be discovered which could affect the content, and all legal disclaimers that apply to the journal pertain.

© 2021 Published by Elsevier B.V.

Journal Pre-proof

NEW CHRONOLOGICAL CONSTRAINTS ON INTENSE HOLOCENE ERUPTIONS AND LANDSLIDE ACTIVITY AT TACANA VOLCANIC COMPLEX (MEXICO)

Jesús Alcalá-Reygosa[a], José Luis Arce[b], José Luis Macías[c], Irene Schimmelpfennig[d], Ricardo Saucedo[e], Juan Manuel Sánchez[f], Teodoro Carlón[c], Rosario Vázquez [g], Guillermo Cisneros-Máximo[c], Adrian Jímenez[h], Salvador Fernández[h], and ASTER Team[d,i]

[a] Facultad de Filosofía y Letras, Universidad Nacional Autónoma de México, Ciudad Universitaria, 04510, Ciudad de México, Mexico. Corresponding author: jalcalar@ucm.es

[b] Instituto de Geología, Universidad Nacional Autónoma de México, Coyoacán, 04510, Ciudad de México, Mexico

[c] Instituto de Geofísica, Universidad Nacional Autónoma de México, Antigua Carretera a Pátzcuaro 8701, 58190, Morelia, Michoacán, Mexico

[d] Aix Marseille Univ, CNRS, IRD, INRAE, Coll France, CEREGE, Aix-en-Provence, France

[e] Instituto de Geología, Universidad Autónoma de San Luis Potosí, San Luis Potosí, México

[f] Instituto Politécnico Nacional-CIIEMAD, Miguel Othón de Mendizábal s/n. Col. La Escalera, C.P. 07320, Del. Gustavo A. Madero, Ciudad de México, Mexico

[g] Escuela Nacional de Estudios Superiores (ENES-Juriquilla), Universidad Nacional Autónoma de Méxic, Campus UNAM Blvd. Juriquilla 3001, Juriquilla, Querétaro, México

[h] Escuela Nacional de Estudios Superiores (ENES-Morelia), Universidad Nacional Autónoma de México, Antigua Carretera a Pátzcuaro 8701, 58190, Morelia, Michoacán, Mexico

[i] Consortium: Georges Aumaître, Didier Bourlès, Karim Keddadouche

Journal Pre-proof

Abstract

Usual methods are unfortunately unsuitable to accurately date many Holocene deposits and landforms from active Mexican volcanoes. This is notably the case for the Tacaná Volcanic Complex (TVC), located in the State of Chiapas in southern Mexico, and the San Marcos Department in Guatemala. The complex consists of the Chichuj, Tacaná, and San Antonio volcanoes and the Ardillas dome. Tacaná volcano, the main summit of the TVC, collapsed 15 ± 5 ka ago ($^{40}Ar/^{39}Ar$), producing the Agua Caliente Debris Avalanche. The result was the formation of a horseshoe-shaped crater 600 m wide open to the northwest. Afterward, several undated effusive and explosive eruptions occurred. All these eruptions are likely Late Pleistocene to Holocene in age because the landforms derived of that activity overlap the horseshoe-shaped crater. To corroborate this hypothesis, we used surface exposure dating with *in situ*-produced cosmogenic ^{36}Cl combined with lichenometry and dendrochronology in the summit domes, the Ardillas dome, the horseshoe-shaped crater's cliff, and a lava. The ^{36}Cl exposure ages (9.3 ± 1.9 ka; 8.9 ± 0.9 ka; 8.6 ± 1.7 ka) of the summit domes are statistically indistinguishable within the associated uncertainties and suggest that the domes formed during Early Holocene. Instead, the southern part of the Late Pleistocene collapsed crater yielded significantly younger ages ranging from 5.3 ± 0.6 to 7.0 ± 0.8 ka. These ages are assumed to be minimum and might indicate later rockfall activity and instability, affecting the horseshoe-shaped crater. The ^{36}Cl exposure age of an andesitic lava (0.4 ± 0.1 ka), emplaced to the SW of Tacaná, is in good agreement with lichenometry (> 347 yr). These ages could represent a gravitational collapse event associated with phreatic explosions vented close to a scar collapse. The ^{36}Cl exposure ages derived from the Ardillas lava dome (0.3 ± 0.1 ka) do not correspond to its emplacement age. The dome must be older than pyroclastic deposits dated at 760 ± 30 yr BP (^{14}C) that cover its surface. Strikingly, the ^{36}Cl, lichenometrical and dendrochronological data of the "Andesitic" lava and the Ardillas dome are associated with NE-SW landslide scars, explosion craters, phreatic vents, fumarolic activity, and tensional fractures. All these features are perpendicular to the NW-SE minimum stress regime (σ3), affecting the TVC and generating gravitational activity. Nowadays, gravitational collapses represent a real threat to the surrounding populations that can be triggered not only by volcanic activity but also by seismicity and extraordinary rains.

Key words: Tacaná, México, *in situ*-produced cosmogenic ^{36}Cl dating, lichenometry, dendrochronology, Holocene.

1. Introduction

Mexican volcanoes have experienced intensive activity during the Holocene, especially in the Trans-Mexican Volcanic Belt, the Chiapanecan Volcanic Arc, the northwestern edge of the Central American Volcanic Arc, Baja California (San Quintin volcanic fields), el Pinacate Volcanic Field (NW Mexico) and the Revillagigedo Archipelago (700 km west of Manzanillo city). Roughly 153 well-constrained Holocene eruptions have been reported of which 63% were produced on active stratovolcanoes and calderas and 37% in monogenetic volcanic fields (Macías and Arce, 2019). To constrain the chronology of these eruptions, several dating methods such as radiocarbon, $^{40}Ar/^{39}Ar$, ^{230}U-Th in zircons, paleomagnetism and *in situ*-produced cosmogenic ^{36}Cl and ^{10}Be have been used (Macías and Arce, 2019). However, many deposits and landforms remain undated, resulting in limitations in the chronological records that prevent establishing highly-resolved histories of volcanic activity to anticipate future eruptions and assess the potential risks for neighboring populations. Such limitations are encountered for Tacaná Volcanic Complex (TVC), located in the State of Chiapas in southern Mexico and the San Marcos Department in Guatemala. Today, more than 300,000 inhabitants live within a 35 km radius of the summit, placing the TVC as the second most hazardous volcano in Mexico, just after Popocatépetl.

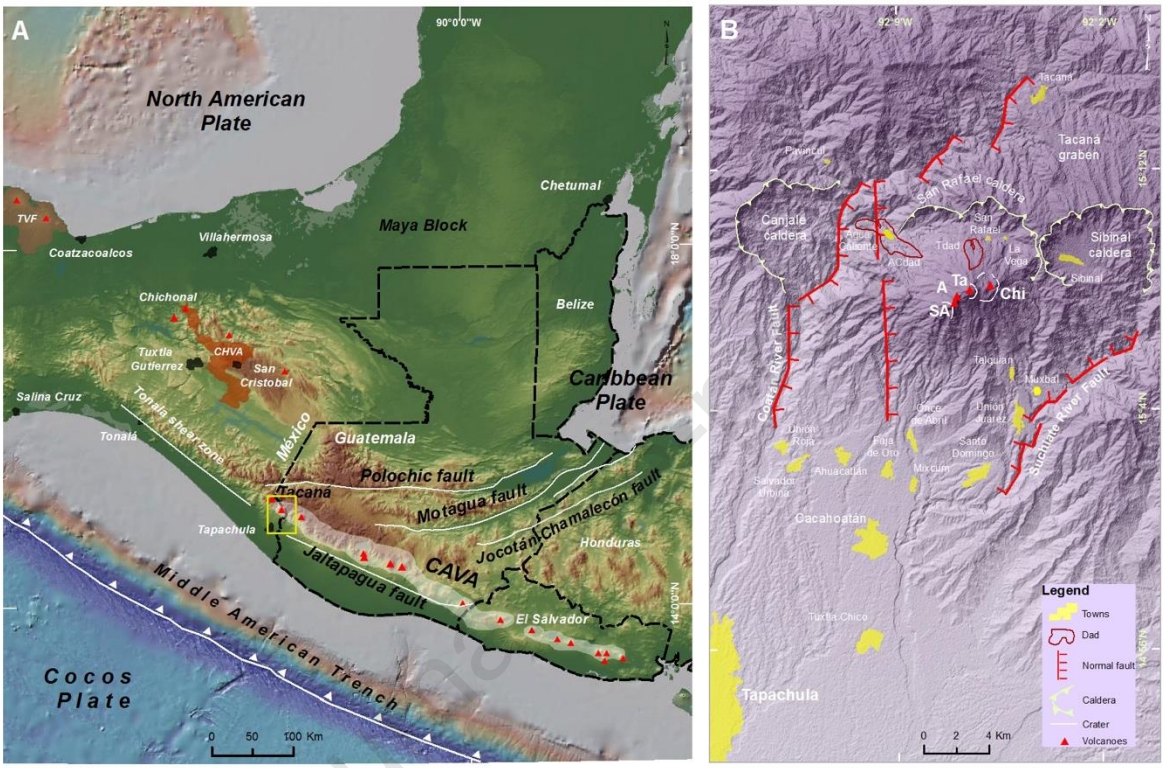
A phreatic explosion occurred at the TVC in 1986 after which it has been considered an active volcano in a quiescent state. The main crater of Tacaná volcano has a horseshoe-shaped crater associated with a collapse event that occurred 15 ± 5 ka ($^{40}Ar/^{39}Ar$) that dispersed the Agua Caliente debris avalanche deposit (Macías et al., 2010). One of the andesitic lavas (Agua Zarca) erupted 12 ± 5 ka ($^{40}Ar/^{39}Ar$) from the collapsed crater and covered the debris avalanche (Macías et al. 2010). These ages are associated with large uncertainties and therefore only provide an approximate chronology of the respective events and tentatively bracket the volcano´s subsequent activity. Besides, little is known about its activity over the Holocene, especially the effusive activity, with several summit

landforms (i.e. domes, lavas) of unknown age. Here, we date four lava domes (three from the Tacaná summit informally dubbed "East", "Northwest" and "Southwest", and the Ardillas dome), the cliff of the horseshoe-shaped crater and a lava (informally named "Andesitic lava") extruded from the summit of Tacaná. We hypothesized that all these landforms have a Late Pleistocene- Holocene age because they overlap the horseshoe-shaped crater dated at 15 ± 5 ka ($^{40}Ar/^{39}Ar$). To confirm this hypothesis, we collected eighteen samples from 5 cm flat-topped solid andesitic surface rocks for exposure dating with *in situ*-produced cosmogenic ^{36}Cl (cosmic ray exposure; ^{36}Cl CRE hereafter) combined with lichenometry and dendrochronology (Ardillas dome and the "Andesitic lava"). The latter two methods provided minimum ages of the sampled rocks. To understand the volcanic evolution of the TVC, we generated a geologic map and stratigraphy of the summit area aided by new structural data. Finally, we performed whole-rock chemistry of all samples to define their chemical composition and evolution of the summit structures.

2. Study area and previous work at Tacaná Volcanic Complex (TVC)

The TVC is part of the northwestern end of the Central American Volcanic Arc (Fig. 1A). The complex is constituted by four NE-SW aligned volcanic structures called Chichuj, Tacaná, Ardillas Dome, and San Antonio (Fig. 1B) (García-Palomo et al., 2006). It was built on Mesozoic metamorphic and Tertiary intrusive rocks (150 Ma and 35-13 Ma respectively), and deposits from mid-Pleistocene calderas (1-2 Ma) (Garduño-Monroy et al., 2015). The complex is affected by three fault systems, which are from older to younger: NW-SE striking fractures and faults that cut the methamorphic and intrusive basement, NE-striking faults parallel to the TVC, and the N-S striking youngest faults that are superimposed on the others (García-Palomo et al., 2006). The NE-SW fault system delimits the Tacaná graben that has controlled the emplacement and evolution of the Chichuj, Tacaná, and San Antonio volcanoes and the Las Ardillas dome structures, as well as the emplacement of Sibinal and San Rafel calderas (Fig. 1B). A linear regression of the alignment of these structures showed an adjustment with a correlation coefficient (r) of

131 0.91, indicating that their location is controlled by N65°E orientation fissures defined by a
132 minimum stress (σ_3) with a N53°W orientation (García-Palomo et al., 2006; Macías et al.,
133 2010).
134



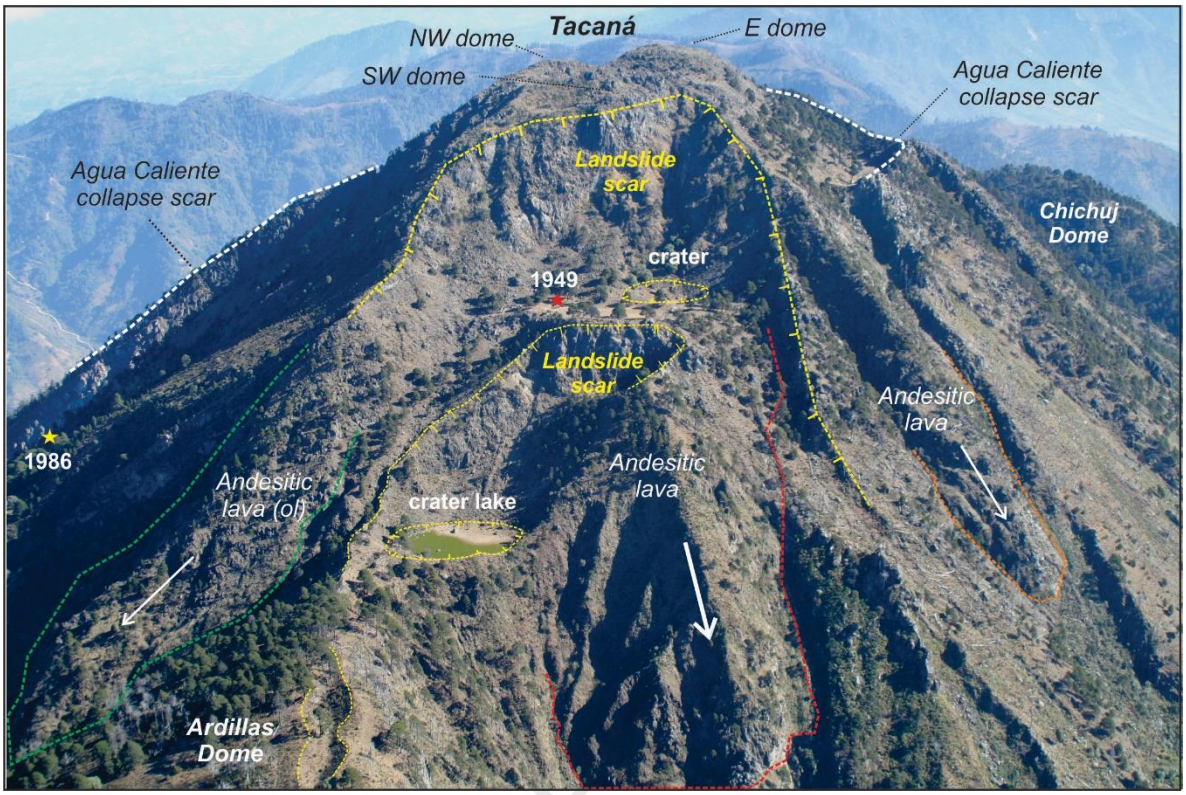
135
136
137 Figure 1. (A) Map showing the tectonic context of southern Mexico and the location of the Tacaná
138 volcanic complex (TVC) (yellow rectangle). Abbreviations: CAVA, Central American Volcanic
139 Arc; TVF, Tuxtlas Volcanic Field; CHVA, Chiapanecan Volcanic Arc. (B) Detailed Digital
140 Elevation Model of the TVC. Abbreviations: Chi (Chichuj), Ta (Tacaná), A (Ardillas dome) and SA
141 (San Antonio) volcanoes; ACdad (Debris Avalanche Deposits of Agua Caliente) and Tdad (Debris
142 Avalanche Deposits of Tuimanj). Main fault systems are displayed in red.
143

144 Volcanic activity in the TVC started ca. 300 ka ago with the emplacement of Chichuj
145 volcano, followed by the emplacement of Tacaná structure around 40 ka (Limón-
146 Hernández, 2011), and San Antonio volcano some ca. 20 ka. Finally, a lava dome defined
147 as Ardillas (>800 yr) was emitted between San Antonio and Tacaná edifices. Since its
148 formation, the TVC has produced several types of eruptions such as sector collapse (Macías
149 et al., 2010), Peléean (Macías et al., 2000), Plinian and subplinian events (Arce et al.,

2012), and intense effusive activity (Limón-Hernández, 2011). As mentioned before, the Tacaná summit has a 600 m wide horseshoe-shaped crater open to the northwest. This crater was produced by a collapse 15 ± 5 ka ago ($^{40}Ar/^{39}Ar$) followed by the emplacement of the Agua Caliente debris avalanche (Macías et al., 2010).

After the collapse, intense effusive activity took place inside the horseshoe-shaped crater through the emission of several lava flows to the NW. One of these lavas called Agua Zarca was dated at 12 ± 5 ka ($^{40}Ar/^{39}Ar$) (Macías et al. 2010). Subsequent lava emissions infilled the horseshoe-shaped crater and extruded the three bulb-like domes ("East", "Northwest", and "Southwest") at the summit of Tacaná (Figs. 2 and 3). Prior or during the first stages of the extrusion of these domes, an olivine-bearing lava flow was emitted to the southwest of Tacaná (green dashed line in Fig. 2). Another lava of andesitic composition was emitted to the southwest between the ca. 15 ka horseshoe-shaped crater and the Ardillas Dome (red dashed line in Fig. 2). These lavas and associated domes have not been dated yet and therefore their relationship with the TVC Holocene eruptive stratigraphy has not been determined. As revealed by stratigraphy and radiocarbon dating, at the beginning of the Holocene an explosive eruption called Once de Abril disrupted the summit of Tacaná, dispersing dense and dilute Pyroclastic Density Currents (PDCs) that swept the volcano flanks beyond the break in slope (Macías et al., 2015). Around the same time, the northern part of Tacaná collapsed producing the Tuimanj debris avalanche towards Guatemala (Limón-Hernández, 2011). Since then, the TVC has generated at least nine radiocarbon dated smaller eruptions that have dispersed pyroclastic deposits on the middle and upper flanks of the complex dated at ca. 7.6, ca. 6.1-5.6, ca. 2.6, ca. 1.9, ca. 0.9, ca. 0.8, ca. 0.37, ca. 0.28, and ca. 0.15 ka (Macías et al., 2015).

Journal Pre-proof



177

178

179 Figure 2. Aerial view from the southwest of the TVC, showing the summit of Tacaná volcano.
180 Notice the Agua Caliente collapse scar (ca. 15 ka), two explosion craters, and two landslide scars
181 (yellow dashed lines). The stars point out the locations of the 1949 (red) and 1986 (yellow) phreatic
182 explosions. The white arrows indicate the flow direction of the andesitic lava analyzed in this study.

183



184

185 Figure 3. Detailed photograph of East, Northwestern and Southwestern lava domes from the summit
186 of Tacaná volcano.

187

188 The precise source of these eruptions is not known yet because the summit has been
189 modified by neotectonics and mass wasting processes. In fact, two NE-SW landslide scars
190 can be recognized at Tacaná (Figs. 2 and 4), one of them is 350 m wide and affects the
191 summit domes; and the second one is 60 m wide and affects the "Andesitic lava" located
192 between the Ardillas dome and the horseshoe-shaped crater, southwest of the summit.
193 Another two NW-SE collapses affect the northwestern part of the Tacaná cone. At least two
194 of the Late Holocene eruptions have occurred along the NE-SW fractures between Tacaná
195 and Las Ardillas dome (Fig. 4). A phreatomagmatic eruption at 760 ± 30 yr cal BP
196 dispersed dilute PDCs and ash fallouts generating a 80 x 60 m wide crater that today
197 contains a greenish lake (Macías et al., 2018). Northeast of this crater lake, at the base of
198 the largest NE-SW scar, another explosion crater vented on top of the "Andesitic lava".
199 This 60 x 25 m wide crater is made of around 5 m thick breccia interbedded with
200 discontinuous pyroclastic deposits (Fig. 2). The 1949 phreatic explosion of Tacaná
201 (Mülleried, 1951) was vented between these two explosion craters and along the NE-SW
202 fractures.
203
204 In 1986, Tacaná resumed activity with another phreatic explosion at the base of a lava cliff,
205 which had formed during the ca.15 ka collapse of Tacaná (Fig. 2). This explosion attracted
206 the attention of scientists (Martini et al., 1987; De la Cruz-Reyna et al., 1989) leading to the
207 discovery of past eruptions (Espíndola et al., 1989) and rise up the awareness of the danger
208 that the volcano represented to the surrounding communities. As a consequence, Mercado
209 and Rose (1992) presented the first general hazards map and mentioned historic reports of
210 another eruption that had occurred around 1855-1856. This eruption has recently been
211 related with the suppression of tree-ring growth between 1857 and 1868 (Carlón et al.,
212 2020).
213
214 Today, the TVC shows signs of volcanic activity with fumaroles on the northwestern flank
215 of San Antonio volcano and thermal springs and fumaroles output on the northwestern
216 flank of Tacaná, which reach as far as the village of Agua Caliente (Rouwet et al., 2004;

2009). On top of the Tacaná summit domes ("East", "Northwest" and "Southwest"), a paleosol is covered by the 1902 ash fall deposits of Santa Maria volcano, Guatemala (Williams and Self, 1983).

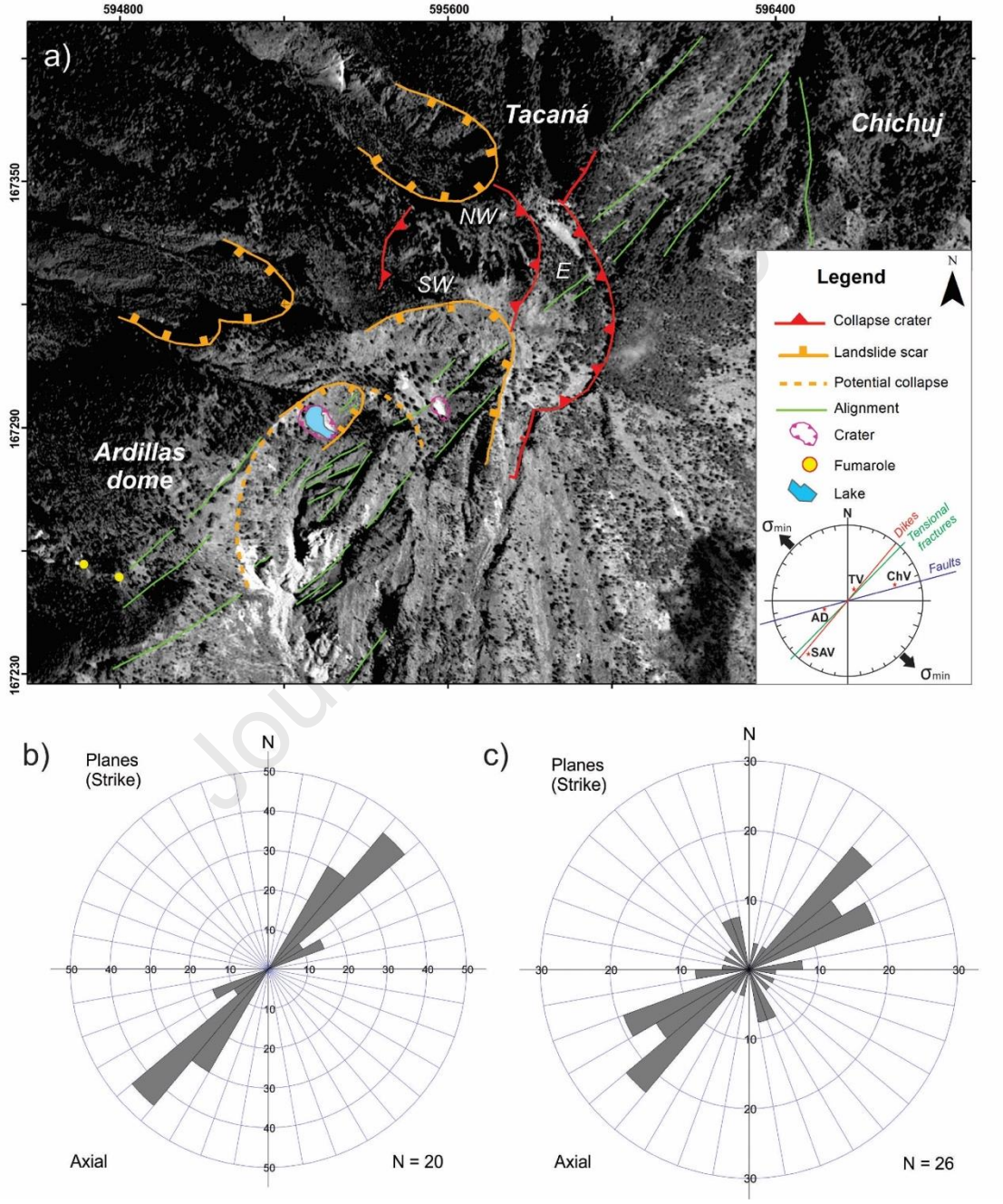


Figure 4. a) Structural map of the TVC summit, b) Rose diagram obtained from the SPOT 7 image and the DEM; c) Rose fracture of the data collected along the NE-SW fracture on top of the San Antonio dome. Dome abbreviations are: E = Eastern, NW = Northwestern, and SW = Southwestern.

3. Methods

3.1. Stratigraphical and structural analyses

The stratigraphic and structural analyses of the area were carried out with a SPOT 7 satellite image, a high resolution Digital Elevation Model (5 m resolution), two Digital Elevation Model (12.5 m resolution, Alospolar, NASA; and 100 m resolution, GeoMapApp.org), and the collection of field data gathered during 2018 and 2019 (Fig. 4a). In specific locations, stratigraphic sections were reconstructed and samples were collected for different analysis.

3.2. Whole-rock chemistry

In this paper, six new chemical analyses for Tacaná summit domes and lavas are reported. Samples were cleaned and washed, then pulverized with a stainless steel mortar. Powder samples were analyzed by the X-ray Fluorescence (XRF) method at Service d'Analyse des Roches et des Minéraux (SARM, CRPG, Nancy, France), major elements by ICP-OES, and trace elements by ICP-MS except Cl (spectrophotometry), B (colorimetry) and Li (atomic absorption). Loss on ignition (LOI) was determined for all analyzed samples, for which 1 gram of powder was heated at 1000°C for one hour and then reweighed.

3.3. Lichenometry

Lichenometry used in this study provides a minimum age of the "Andesitic lava" and the Ardillas dome. The largest diameter of the biggest circular thalli of *Rhizocarpon geographicum* located on well preserved protruding features with smooth surfaces were measured using a Bernier calibrator. Digital photographs of the lichen were taken, using a scale (one peso coin of 21 mm of diameter). The age of the largest lichen was determined applying the growth rate of 0.23 mm a^{-1} for *Rhizocarpon geographicum* constrained on Iztaccíhuatl volcano, situated ca. 900 km to the northwest of the TVC (Palacios et al., 2012). Despite the distance, the measurement sites of the lichen are located at a similar

altitude (~4,000-4,500 m a.s.l.), and climate at that altitudinal range is not significantly different on both volcanoes.

3.4. Dendrochronological sampling and sample processing

Dendrochronological samples were collected from *Pinus hartwegii* Lindl (9 samples) and *Juniperus monticola* (1 sample) on the summits of the Tacaná volcano and Ardillas dome in the years 2017 and 2019. No samples of trees were collected on the "Andesitic lava", because continuous landslides limit their colonization. The sampled trees were located at elevations ranging from 3400 to 4040 m. The sampling consisted in extracting two or three increment cores from each tree using a Häglof borer (10 mm diameter; Häglof Sweden AB, Långsele, Västernorrland, Sweden) perpendicular to the stem and at breast height (1.30 m). Then, 10 trees were drilled for a total sampling set of 22 increment cores. Increment cores were processed using sandpaper with progressive grain sizes from 80 to 1200 grains·cm^{-2} according to standard dendrochronological techniques (Stokes and Smiley, 1996). Once the annual rings were visible, growth rings were counted from the pit to the bark under the microscope.

3.5. Cosmic ray exposure dating with ^{36}Cl

In Mexico, CRE dating has been previously used to determine the age of lavas (Vázquez-Selem and Heine, 2011; Alcalá-Reygosa et al., 2018 a, b) and domes (Arce et al., 2003) in stratovolcanoes and monogenetic edifices. CRE dating relies on the interaction of cosmic ray derived particles with certain target elements of the rocks. ^{36}Cl can be extracted from any mineral phase and rock type that contains one or more of its most important target elements, i.e. Ca, K and Cl (Dunai, 2010). Moreover, it has been recently demonstrated that ^{36}Cl dating provides surface exposure ages of volcanic rocks of as young as a few hundred years (Jomelli et al., 2016).

3.5.1. Sampling and physical treatment of the samples

Eighteen samples (Tac 1 - Tac 18) were taken with hammer and chisel from the 5 cm flat-topped solid rock surfaces (Table 1). Twelve of them were collected on the "East", "Northwest" and "Southwest" Tacaná domes (Tac 1 - Tac 9) and the Ardillas dome (Tac 13 - Tac 15). Three samples were taken from the limit of the steep cliff of the horseshoe-

shaped crater (Tac 10 - Tac 12) and another three come from the "Andesitic lava" located to the southwest of this crater (Tac 16 - Tac 18). All the samples were collected from well-preserved surfaces without evidence of erosion, weathering or boulder toppling to minimize potential bias in the ^{36}Cl surface concentrations, which accumulated during exposure to cosmic rays since formation of the sampled surfaces (Alcalá-Reygosa et al., 2018a). Furthermore, samples were collected from protruding geometries to minimize the effects of surface shielding by pyroclastic layers and soils. The geographic coordinates were obtained with Garmin GPS, and the topographic shielding was determined with compass and clinometer. It must be noted that the samples taken from the steep cliff of the horseshoe-shaped crater, Las Ardillas dome and the "Andesitic lava" represented a challenge due to active gravitational processes, neotectonics and slope instability, which could compromise our original plan to determine the ages of the landforms.

Sample	Latitude (°N)	Longitude (°W)	Altitude (m.a.s.l)	Thickness (cm)	Shielding factor
Tac 1	15.13	-92.10	4086	2.0	0.98665
Tac 2	15.13	-92.10	4097	2.0	0.99343
Tac 3	15.13	-92.10	4102	2.5	0.97627
Tac 4	15.13	-92.10	4081	4.0	0.99637
Tac 5	15.13	-92.10	4088	2.0	0.99718

Journal Pre-proof

Tac 6	15.13	-92.10	4081	2.0	0.97541
Tac 7	15.13	-92.10	4079	2.5	0.99977
Tac 8	15.13	-92.10	4077	2.0	0.99687
Tac 9	15.13	-92.10	4089	2.5	0.99858
Tac 10	15.13	-92.10	3958	1.5	0.99129
Tac 11	15.13	-92.10	3986	1.5	0.98564
Tac 12	15.13	-92.10	3995	1.5	0.95418
Tac 13	15.12	-92.11	3792	1.5	0.95905
Tac 14	15.12	-92.11	3764	1.5	0.98316
Tac 15	15.12	-92.11	3755	1.0	0.97223
Tac 16	15.12	-92.11	3898	1.5	0.92531
Tac 17	15.13	-92.11	3887	1.5	0.95965
Tac 18	15.13	-92.11	3929	3.0	0.87414

Table 1. Field data and characteristics of rock samples from lava domes, cliff horse-shoe shaped crater and lava from Tacaná volcano, used for the ^{36}Cl CRE dating calculations. The shielding factor was obtained using the Topographic Shielding Calculator v2.0 provided by CRONUS-Earth Project (2014).

At Instituto de Geofísica (Unidad Morelia; Universidad Nacional Autónoma de México), lichens, mosses and other organic matter were removed from the samples with a brush and then they were crushed with a roller grinder and sieved to retrieve the grain size fraction (0.25-0.50 mm). Once the crushed samples shipped to the Centre Européen de Recherche et d'Enseignement des Géosciences de l'Environnement (CEREGE; France), aliquots of the bulk rock were first taken for the analysis of the major and trace element concentrations at the "Service d'Analyse des Roches et des Minéraux" (SARM, CRPG, Nancy, France), which are needed to estimate the samples ^{36}Cl production rate from the capture of the low-energy neutrons by Cl in the samples (Table 2). This specific ^{36}Cl production reaction is difficult to constrain and associated with significant uncertainties (Schimmelpfennig et al., 2009). As feldspar phenocrysts often contain significantly less Cl than volcanic whole rock

samples (Schimmelpfennig et al., 2009), the proportion of the non-magnetic feldspar in the fraction of the sample grains used for ^{36}Cl extraction was increased by discarding the most magnetic minerals with a magnetic separator "Frantz LB-1" at CEREGE. However, because feldspars were not abundant enough, pure feldspar was not used to avoid the risk of too small sample masses with ^{36}Cl contents below the detection limit.

3.5.2. Chemical sample treatment and measurement

Between 20 and 100 g of the feldspar-enriched sample fractions (Tac 1 - Tac 18) were treated for ^{36}Cl extraction following the method described in Schimmelpfennig et al. (2011). The samples were washed in ultrapure water to remove fine-grained powder and then leached in a dilute HF/HNO_3 mixture to dissolve 15 - 20 % of the initial sample mass. Thus, the samples were decontaminated from atmospheric ^{36}Cl and potentially Cl-rich groundmass grains were reduced (Schimmelpfennig et al., 2009). Then, the samples were dried and 2 g aliquots of each sample were put aside for analysis of the major elements at SARM, because Ca, K, Ti, and Fe are the target elements for spallogenic/muogenic production of ^{36}Cl (Table 3). The following steps consisted in adding a ^{35}Cl-enriched spike (~ 99%) to each sample and dissolving totally them in a HF/ HF/HNO_3 mixture. A chemistry blank was processed following the same protocol as the samples.

After total dissolution, the samples were centrifuged to discard the undissolved residues and gel (fluoride complexes, CaF_2). Then, chlorine in the liquid solution was precipitated to silver chloride (AgCl) by adding 2 ml of a silver nitrate ($AgNO_3$) solution at 10%. To allow the AgCl to settle down on the bottom of the bottles, samples were stored for 2 days in a dark place. This enabled the extraction of the supernatant solution (excess HF and HNO_3) by a peristaltic pump avoiding the disturbance of the AgCl precipitate. In the next step, aiming to reduce the isobaric interferences of ^{36}S throughout the ^{36}Cl measurements by Accelerator Mass Spectrometry (AMS), sulphur was removed in the form of barium sulphate ($BaSO_4$) obtained after the re-dissolution of this first AgCl precipitate and the addition of 1 ml of a saturated solution of barium nitrate ($Ba(NO_3)_2$). $BaSO_4$ was discarded by centrifuging and filtering the supernatant with a syringe and an acrodisc filter. Then,

AgCl was precipitated again with 3-4 ml of diluted HNO_3 (1:1 vol.). The precipitate was collected after centrifuging, was rinsed and finally dried in the oven at 80 ºC for 2 days, and later loaded into nickel cathodes for measurements of the $^{36}Cl/^{35}Cl$ and $^{35}Cl/^{37}Cl$ ratios by AMS isotope dilution at the French national AMS facility ASTER (CEREGE, France) (Arnold et al., 2013), which took place in 2019. The $^{36}Cl/^{35}Cl$ ratio was normalized to in-house standard SM-CL-12 with an assigned $^{36}Cl/^{35}Cl$ ratio of (1.428 ± 0.021) $x10^{-12}$ (Merchel et al., 2011), and regarding the $^{35}Cl/^{37}Cl$ ratio, a natural ratio of 3.127 was assumed. The AMS analytical data is given in Table 4.

3.5.3. *In situ*-produced ^{36}Cl age calculation

We calculated the ^{36}Cl CRE ages using the Excel spreadsheet published by Schimmelpfennig et al. (2009). We used the following ^{36}Cl production rates and parameters referenced to sea level and high latitude based on the time-invariant "St" scaling (Stone, 2000): 42.2 ± 4.8 atoms ^{36}Cl $(g\ Ca)^{-1}$ yr^{-1} for spallation of Ca (Schimmelpfennig et al., 2011); 148.1 ± 7.8 atoms ^{36}Cl $(g\ K)^{-1}$ yr^{-1} for spallation of K (Schimmelpfennig et al., 2014); 13 ± 3 atoms ^{36}Cl $(g\ Ti)^{-1}$ yr^{-1} for spallation of Ti (Fink et al., 2000); 1.9 ± 0.2 atoms ^{36}Cl $(g\ Fe)^{-1}$ yr^{-1} for spallation of Fe (Stone et al., 2005), and 696 ±185 neutrons $(g\ air)^{-1}$ yr^{-1} at the Earth's surface/atmosphere interface for the production rate of epithermal neutrons from fast neutrons in the atmosphere (Marrero et al., 2016). Both the nucleogenic and muonic scaling factors were determined using the time-invariant scaling model of Stone (2000) based on CosmoCalc (Vermeesch, 2007) and the atmosphere standard model (N.O.A.A., 1976). High-energy neutron attenuation length of 160 g cm^{-2} was used. A density of 2.5 g/cm^3 is assumed for all samples.

The topographic shielding factor was estimated applying the Topographic Shielding Calculator v2.0 provided by CRONUS web calculator. The ^{36}Cl CRE ages are presented without erosion and snow cover corrections. Regarding erosion, all the sampled surfaces are well-preserved whereas potential snow cover effects were not considered because snowfall is very rare in this tropical climate.

4. Results

4.1. Structural setting and stress regime

The structural data is presented in figure 4a and plotted in rose diagrams on figures 4b-c. The performed image analyses and field reconnaissance revealed the occurrence of elongated rhombic large scale fractures on top of Las Ardillas dome with a preferential direction between N30°E to N70°E (Figs. 2 and 4b). These fractures have a NE-SW main axis. Their SW tip ends in a hydrothermal alteration zone with fumaroles on the northern flank of San Antonio volcano and their NE tip is connected with the two NE-SW landslide scars. Along these rhombic fractures occurred the 1949 phreatic explosion, signs of hydrothermal fluid paths, and the two explosion craters described in figures 2 and 4. The structural analysis of field data in andesitic rocks shows a preferential fracturing system with a N40°E to N70°E orientation and a secondary one with NNW-SSE direction (Fig. 4c). Analysis of all these data allows defining a stress regime atop the TVC represented by a minimum main stress (σ_3) with a N40°W± 10° orientation.

4.2. Cosmogenic ^{36}Cl chronology, lichenometry and dendrochronology.

In Table 4, the ^{36}Cl CRE ages are given with their full uncertainties, i.e. including analytical and production rate errors, as well as with their analytical errors only. In the text and figures, individual sample ages are shown with their analytical errors only, while arithmetic mean ages are given with their standard deviations. The age population from each dated volcanic feature was tested for outliers using the χ^2 test of Ward and Wilson (1978). The individual ^{36}Cl ages range between 11.0 ± 1.8 ka and 170 ± 70 years. Most of the sample fractions that were little enriched in feldspar (see section 3.5.1), have high natural Cl concentrations (up to ~265 ppm), while Cl concentrations as low as 13 ppm were obtained in sample fractions with a high feldspar proportion. This led to ~10-65%

429 contributions from Cl-derived ^{36}Cl to the total ^{36}Cl production and associated uncertainties
430 in resulting ages of up to ~22% (Table 2 and 3).
431
432 **4.2.1. Tacaná summit domes**
433
434 The summit "East", "Northwest" and "Southwest" lava domes are hosted within the 600 m
435 wide horseshoe-shaped crater of Tacaná that is breached to the northwest (Figs. 2 and 3).
436 They have a bulby shape, with three recognizable lobes. Together these domes occupy an
437 area of 0.18 km^2, with a radius of approximate 300 m, and correspond to a volume of 0.017
438 km^3. The highest dome ("East dome") has an elevation of 4060 m a.s.l. It rises 87 m above
439 the surrounding terrain and holds an older microwave antenna. This dome is separated from
440 the "Northwest" and "Southwest" domes by a N-S fault scar. The western lava lobes reach
441 a maximum elevation of 3990 m and they are not easily distinguished from the Eastern
442 dome.
443
444 The summit of the "Northwest" and "Southwest" domes are separated by a 15 m depression
445 in north-south direction. The "Southwest" dome emplaced an olivine-bearing lava to the
446 southwest, and both are affected by the large NE-SW scar open to the southwest. The
447 "Southwest" and the "Northwest" domes have an andesitic composition of 62.48 wt.% SiO_2
448 and 62.65 wt.% SiO_2, respectively. A dacitic composition with 63.6 wt.% SiO_2 (on
449 anhydrous basis) has been evidenced on the "East" dome (Fig. 5a). The olivine-bearing
450 lava is the most mafic lava analyzed. It is andesitic in composition (Fig. 5a) with 57.5 wt.%
451 SiO_2 that falls close to the basaltic andesitic field.
452

Sample	Samples calculated with this composition	Unit	SiO_2	TiO_2	Al_2O_3	Fe_2O_3	MnO	MgO	CaO	Na_2O	K_2O	P_2O_5	LOI	Total	Li	Sm	Gd	Cl	U	Th
*Tac0911	-	PreCL	60.27	0.64	17.11	6.48	0.11	2.36	5.98	3.78	2.23	0.17	0.27	99.40	-	-	-	-	-	3
*Tac0808	-	AndL	59.51	0.66	18.03	6.54	0.12	2.67	6.23	3.64	2.08	0.19	0.23	99.90	-	-	-	-	-	4
*Tac0829E	-	ME	53.69	0.95	18.56	8.53	0.12	4.06	8.36	3.58	1.23	0.20	0.21	99.49	-	-	-	-	-	3
*Tac0829L	-	AndL	61.13	0.57	16.83	5.73	0.10	2.42	5.62	3.71	2.23	0.15	1.38	99.87	-	-	-	-	-	4
*Tac0829a	-	AndL	62.27	0.59	16.83	5.60	0.10	2.21	5.40	3.80	2.32	0.16	0.35	99.63	-	-	-	-	-	4

Sample	CaO (%)	K_2O (%)	TiO_2 (%)	Fe_2O_3 (%)	SiO_2 (%)	Na_2O (%)	MgO (%)	Al_2O_3 (%)	MnO (%)

*Tac0827	-	PreCL	58.70	0.61	16.67	6.15	0.11	2.52	5.70	3.62	2.13	0.16	3.23	99.60	-	-	-	-	-	4
*Tac0823	-	And-Ol	57.28	0.80	17.74	7.25	0.11	3.88	7.21	3.59	1.68	0.17	0.08	99.79	-	-	-	-	-	3
*Tac0809	-	Dome	60.77	0.64	17.38	6.23	0.11	2.63	5.96	3.69	2.15	0.17	0.23	99.96	-	-	-	-	-	3
*Tac0811	-	Dome	62.61	0.56	16.69	5.57	0.10	2.30	5.41	3.69	2.38	0.16	0.24	99.71	-	-	-	-	-	3
**Tac9878	-	Dome	62.78	0.55	16.88	5.26	0.10	2.17	5.34	3.70	2.32	0.15	0.80	100.05	-	-	-	-	-	-
***Tac9863	-	ArD	62.96	0.58	16.76	4.82	0.11	2.42	5.74	3.82	2.06	0.13	0.60	100.00	-	4.2	-	-	2.8	4.7
[1]TAC-1	Tac 2, 3	Dome	61.25	0.62	16.22	6.05	0.11	2.46	5.22	3.65	2.31	0.15	1.12	99.16	24	3.3	2.8	300	1.4	4.35
[1]TAC-4	Tac 5, 6	Dome	61.98	0.62	15.50	6.08	0.11	2.52	4.72	3.52	2.27	0.13	1.96	99.40	24	3.2	2.7	280	1.4	4.28
[1]TAC-7	Tac 8, 9	Dome	61.42	0.61	16.16	5.75	0.11	2.59	5.28	3.62	2.34	0.14	1.34	99.36	25	3.1	2.7	370	1.5	4.23
[1]TAC-10	Tac 11, 12	PreCL	61.16	0.64	16.19	6.80	0.13	2.41	5.07	3.59	2.38	0.17	0.65	99.19	21	3.1	2.7	72	1.5	4.16
[1]TAC-13	Tac 14, 15	ArD	64.53	0.53	15.75	5.07	0.10	2.07	4.52	3.74	2.72	0.14	0.44	99.61	25	2.9	2.5	335	1.7	5.01
[1]TAC-16	Tac 17, 18	AndL	64.36	0.51	15.83	4.72	0.09	1.87	4.55	3.73	2.65	0.14	0.72	99.16	24	2.8	2.4	320	1.7	5

Table 2. Major and trace element concentrations in bulk rock samples from Tacaná Volcanic Complex, before chemical treatment (see methods). We used the composition of one sample per landform for the age calculations of all other samples from the same feature, assuming that variations in compositions are insignificant. LOI, loss on ignition; total Fe as Fe_2O_3. Compiled samples from Tacaná summit: *Limón-Hernández (2009). Units are: PreCL, Pre-colapse lava; AndL, Andesitic lava; ME, Mafic enclave; And-Ol, olivine-bearing andesitic lava; ArD, Ardillas dome. References: **Mora et al. (2004); ***García-Palomo et al. (2006); [1]This work.

Journal Pre-proof

Eastern lava dome									
Tac 1	6.08 ± 0.30	1.94 ± 0.10	0.32 ± 0.08	3.07 ± 0.46	62.71	4.04	2.12	18.09	0.08
Tac 2	5.52 ± 0.28	1.78 ± 0.17	0.26 ± 0.05	2.54 ± 0.38	65.35	3.66	1.68	16.60	0.07
Tac 3	6.21 ± 0.31	1.90 ± 0.40	0.31 ± 0.07	2.98 ± 0.45	62.49	4.09	2.10	18.38	0.08
Northwestern lava dome									
Tac 4	8.33 ± 0.42	0.60 ± 0.12	0.06 ± 0.02	0.65 ± 0.09	60.40	4.59	0.21	22.66	0.02
Tac 5	6.38 ± 0.32	1.43 ± 0.28	0.22 ± 0.05	2.05 ± 0.31	63.36	3.89	1.43	18.31	0.06
Tac 6	6.75 ± 0.33	1.32 ± 0.13	0.21 ± 0.05	2.18 ± 0.33	61.63	4.11	1.41	19.58	0.06
Southwestern lava dome									
Tac 7	9.14 ± 0.46	0.60 ± 0.15	0.05 ± 0.01	0.58 ± 0.09	57.21	5.25	0.18	25.29	0.02
Tac 8	6.41 ± 0.32	1.82 ± 0.36	0.29 ± 0.07	2.53 ± 0.38	62.07	4.18	1.76	18.69	0.07
Tac 9	6.78 ± 0.34	1.66 ± 0.33	0.25 ± 0.06	2.20 ± 0.33	61.66	4.38	1.62	19.77	0.06
Cliff horse-shoe shaped crater									
Tac 10	6.76 ± 0.34	1.47 ± 0.29	0.24 ± 0.05	2.73 ± 0.41	61.68	4.21	1.27	19.86	0.07
Tac 11	9.52 ± 0.48	0.45 ± 0.09	0.04 ± 0.01	0.54 ± 0.08	57.43	5.15	0.08	25.73	0.02
Tac 12	6.82 ± 0.34	1.33 ± 0.26	0.19 ± 0.05	2.64 ± 0.40	62.23	4.11	1.77	19.63	0.08
Ardillas lava dome									
Tac 13	7.44 ± 0.37	1.37 ± 0.18	0.23 ± 0.06	2.16 ± 0.22	60.37	4.50	1.54	21.05	0.06
Tac 15	6.71 ± 0.33	1.69 ± 0.17	0.26 ± 0.06	2.47 ± 0.25	61.95	4.33	1.79	19.79	0.07
Andesitic lava									
Tac 16	7.43 ± 0.37	1.32 ± 0.13	0.24 ± 0.06	2.14 ± 0.21	60.52	4.51	1.50	21.06	0.06
Tac 17	7.32 ± 0.37	1.35 ± 0.13	0.34 ± 0.08	3.29 ± 0.33	59.43	4.24	2.47	19.64	0.09
Tac 18	7.46 ± 0.37	1.28 ± 0.13	0.20 ± 0.05	1.94 ± 0.19	59.97	4.55	1.32	21.21	0.05

Table 3. Concentrations of the major elements, including the ^{36}Cl target elements Ca, K, Ti and Fe, measured in splits taken from the samples after magnetic separation and the chemical pre-treatment. Analyses carried out at Service d'Analyse des Roches et des Minéraux (SARM, CRPG, Nancy, France) by ICP-OES.

Journal Pre-proof

Sample	Sample weight (g)	Mass Cl (mg) added by spike	^{35}Cl / ^{37}Cl	^{36}Cl / ^{35}Cl (10^{14})	Cl (ppm)	^{36}Cl conc (10^{3} at g^{-1})	^{36}Cl age (ka)
Eastern lava dome							
Tac 1	66.87	2.016	3.595 ± 0.043	26.9 ± 1.4	265 ± 38	1060 ± 150	9.7 ± 2.1 (1.4)
Tac 2	76.12	2.009	3.712 ± 0.045	21.9 ± 1.3	185 ± 25	621 ± 80	7.3 ± 1.5 (1.0)
Tac 3	79.13	2.013	3.524 ± 0.042	31.5 ± 1.7	263 ± 40	1210 ± 180	11.0 ± 2.5 (1.8)
Northwestern lava dome							
Tac 4	25.77	2.010	8.53 ± 0.10	21.6 ± 1.3	57 ± 7	449 ± 32	9.7 ± 1.4 (1.0)
Tac 5	59.54	2.012	3.841 ± 0.046	22.4 ± 1.2	194 ± 25	690 ± 82	8.0 ± 1.6 (1.1)
Tac 6	40.6	2.018	4.574 ± 0.054	23.4 ± 1.3	140 ± 17	622 ± 61	8.9 ± 1.6 (1.0)
Southwestern lava dome							
Tac 7	19.7	2.019	8.66 ± 0.53	18.8 ± 2.0	73 ± 11	507 ± 60	9.8 ± 1.7 (1.3)
Tac 8	82.81	2.003	3.625 ± 0.043	20.6 ± 1.2	200 ± 28	615 ± 84	6.7 ± 1.4 (1.0)
Tac 9	60.73	2.013	3.736 ± 0.044	27.0 ± 1.4	224 ± 30	931 ± 115	9.4 ± 2.0 (1.3)
Cliff horse-shoe shaped crater							
Tac 10	55.27	2.019	9.62 ± 0.11	22.4 ± 1.3	22 ± 3	205 ± 14	5.29 ± 0.72 (0.64)
Tac 11	14.68	2.015	34.75 ± 0.43	1.08 ± 0.20	13 ± 2	22.2 ± 6.5	0.66 ± 0.21 (0.20)
Tac 12	58.8	2.009	7.109 ± 0.084	26.8 ± 1.4	34 ± 4	276 ± 20	6.99 ± 0.95 (0.81)
Ardillas lava dome							
Tac 13	69.06	2.056	3.789 ± 0.045	0.88 ± 0.20	185 ± 24	24.2 ± 6.3	0.339 ± 0.102 (0.099)
Tac 14	30.79	2.008	10.60 ± 0.13	0.140 ± 0.063	33 ± 4	-	-
Tac 15	63.5	2.022	3.866 ± 0.046	0.46 ± 0.15	177 ± 23	11.8 ± 4.4	0.169 ± 0.069 (0.065)
Andesitic lava							
Tac 16	50.98	2.043	4.078 ± 0.048	1.18 ± 0.24	172 ± 22	32.9 ± 7.8	0.47 ± 0.13 (0.11)
Tac 17	53.27	2.040	4.039 ± 0.048	0.79 ± 0.19	172 ± 22	21.2 ± 6.0	0.294 ± 0.092 (0.085)
Tac 18	61.72	2.027	3.931 ± 0.047	1.15 ± 0.23	167 ± 21	30.0 ± 7.1	0.44 ± 0.13 (0.11)
Blank 01	-	2.002	116.4 ± 1.5	0.23 ± 0.16	-	-	-

Table 4. Analytical ^{36}Cl data and resulting ^{36}Cl CRE ages for samples from Tacaná Volcanic Complex. Age uncertainties (1σ) include production rate errors as well as analytical errors; numbers in parenthesis correspond to analytical errors only.

Journal Pre-proof

Figure 6 and Table 4 (also supplement material) present the nine ^{36}Cl CRE ages calculated from the samples collected at the summit lava domes "East", "Northwest" and "Southwest" of Tacaná volcano. On the "East" dome, samples Tac-1, -2 and -3 lead to ^{36}Cl CRE ages of 9.7 ± 1.4 ka, 7.3 ± 1.0 ka, 11.0 ± 1.8 ka, respectively. Considering their associated uncertainties, they are statistically indistinguishable and lead to an arithmetic mean ^{36}Cl CRE age and standard deviation of 9.3 ± 1.9 ka. On the "Northwest" dome, the calculated ^{36}Cl CRE ages of 9.7 ± 1.0 ka, 8.0 ± 1.1 ka and 8.9 ± 1.0 (samples Tac-4, -5 and -6) lead to an arithmetic mean ^{36}Cl CRE age of 8.9 ± 0.9 ka, whereas on the "Southwest" dome, the calculated ^{36}Cl CRE ages of 9.8 ± 1.3 ka, 6.7 ± 1.0 ka and 9.4 ± 1.3 ka (samples Tac-7, -8, and -9) lead to an arithmetic mean ^{36}Cl CRE age of 8.6 ± 1.7 ka. Dendrochronological data around the summit area lead to tree ages ranging from 83 to 164 years. The youngest trees are located on the summit of Tacaná dome (83 years, A1, *Juniperus monticola*) at 4058 m a. s. l. A similar age (<100 years) from the thali of *Rhizocarpon geographicum* is obtained.

4.2.2. Horseshoe-shaped crater of Tacaná volcano

Remnant lavas from the horseshoe-shaped crater of Tacaná are distributed to the south, east and southeast of the main Tacaná edifice (Figs. 2 and 6). As mentioned before, the 600 m wide crater breached to the NW was produced by the 15 ± 5 ka collapse. Samples from these lavas, which were analyzed in this work, have an andesitic composition (60 wt.% SiO_2) with 6 wt.% alkalies (Fig. 5a). Furthermore, the three samples for ^{36}Cl CRE dating from the southern edge of the horseshoe-shaped crater (samples Tac-10, -11 and -12) lead to ^{36}Cl CRE ages of 5.3 ± 0.6 ka, 0.7 ± 0.2 ka and 7.0 ± 0.8 ka, respectively (Fig. 6, Table 4 and supplement material).

4.2.3. "Andesitic lava"

The "Andesitic lava" was vented at the base of the "Southwest" dome of Tacaná and at the large NE-SW horseshoe-shaped crater (Figs. 2 and 6). Three samples from these lavas that hosted basaltic andesite mafic enclaves were collected. The geochemical analysis of pure lava samples have an andesitic composition varying from 59 to 62 wt.% SiO_2, although one sample lies at the limit between andesite and dacite compositions (63 wt.% SiO_2, on

anhydrous basis) (Fig. 5a; Table 2). The lava composition is similar to that from the "Southwest" dome and periphery lavas (Fig. 5b-g) and the sampled mafic enclaves are similar to other enclaves reported in previous works (Mora et al., 2004; 2013). Besides, the three ^{36}Cl CRE ages from these "Andesitic" lava samples Tac 16, 17, 18 are 0.5 ± 0.1 ka, 0.3 ± 0.1 ka and 0.4 ± 0.1 ka, respectively (Fig 6, Table 4 and supplement material). Considering their associated uncertainties, they are statistically indistinguishable and lead to a mean ^{36}Cl CRE age of 0.4 ± 0.1 ka. Furthermore, lichenometry lead to a minimum age of 390 years (Fig. 7).

4.2.4. Las Ardillas dome

The chemical analyses of two samples from the Ardillas dome (Table 2) complemented with one sample from a previous work (García-Palomo et al., 2006) indicate that the Ardillas dome is the most silicic structure of the TVC. It is dacitic in composition (Fig. 5a) with silica contents of 63-65 wt.% and alkalies of 5.8-6.5 wt.%. All the samples have the lowest values in MgO, CaO, Fe_2O_3, and Al_2O_3 (Fig. 5b-g), according to their more evolved character (more silica rich). Figure 6 and Table 4 (also supplement material) present the ^{36}Cl CRE ages of the Ardillas lava dome, which are 0.3 ± 0.1 ka and 0.2 ± 0.1 ka (Tac-13 and -15) and lead to a mean ^{36}Cl CRE age of 0.3 ± 0.1 ka. Due to the number of ^{36}Cl atoms determined by AMS for sample Tac 14 being similar to that determined for the chemically processed blank considering their associated analytical uncertainties, it is not possible to calculate an exposure age for this sample. However, its ^{36}Cl concentration close to the chemical blank value indicates a very short exposure duration. On top of the Ardillas dome, the tree ages range from 117 to 164 years, whereas trees closer to the eastern vertical wall of the dome have ages ranging from 117 to 138 years (supplement material). In addition, lichenometry provides a minimum age of 300 years (Fig. 7).

Journal Pre-proof

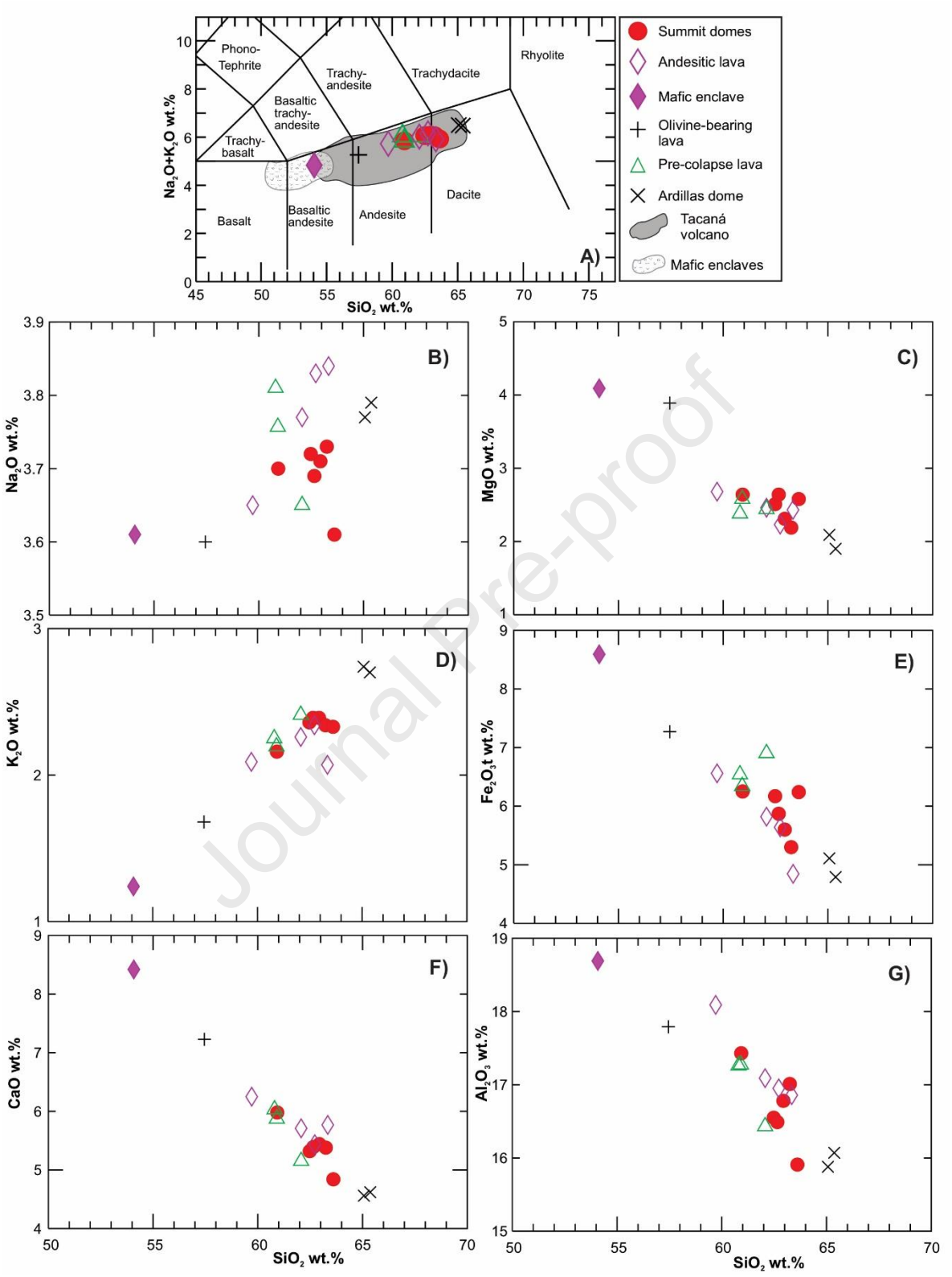
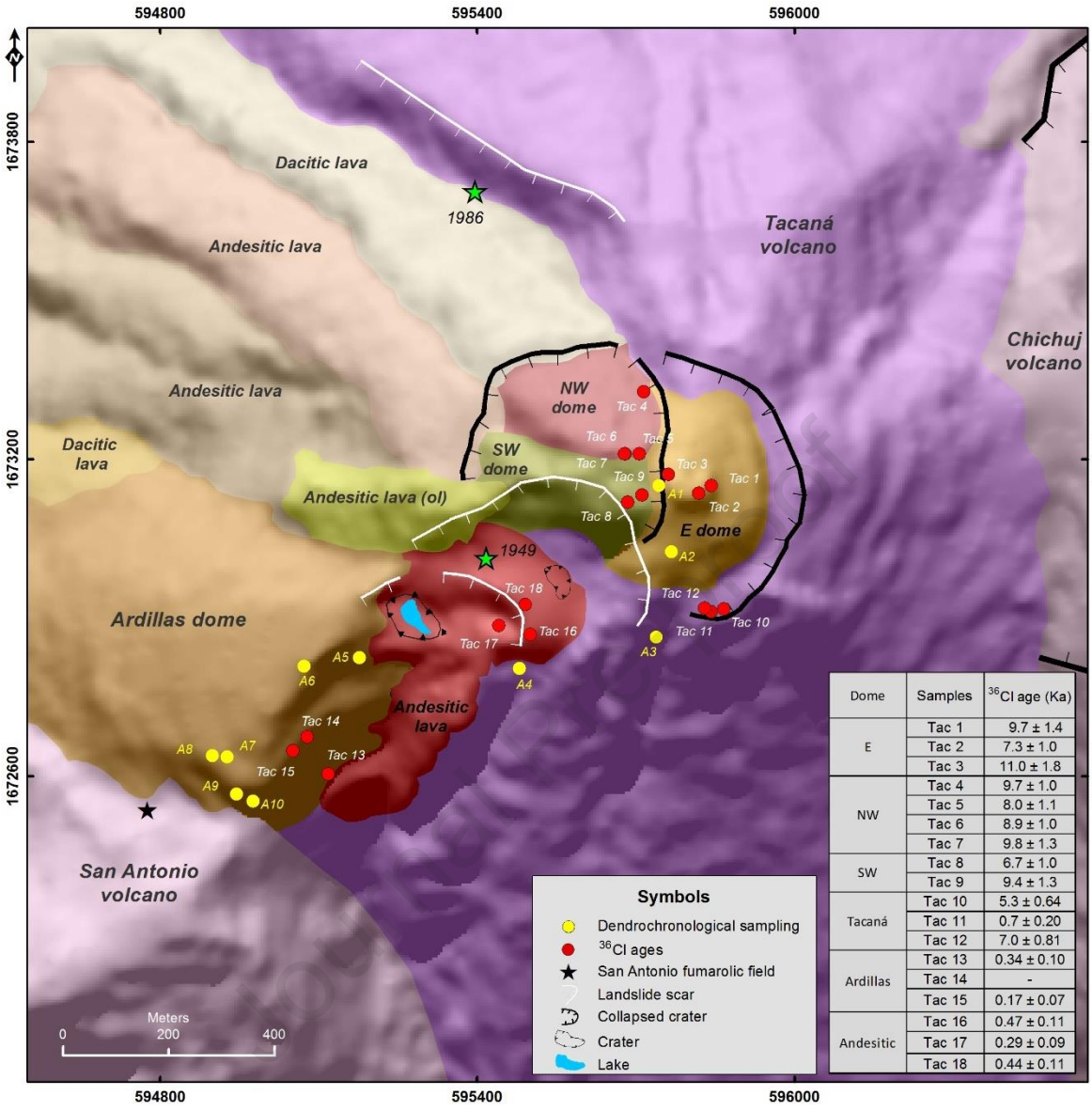


Figure 5. Whole-rock chemical composition of Tacaná samples. A) Total alkalies vs silica diagram (Le Bas et al., 1986) and B-G) binary diagrams. All samples were plotted on anhydrous basis. Gray and dotted areas were taken from previous works (Mora et al., 2004; Arce et al., 2015).



Dome	Samples	^{36}Cl age (Ka)
E	Tac 1	9.7 ± 1.4
	Tac 2	7.3 ± 1.0
	Tac 3	11.0 ± 1.8
NW	Tac 4	9.7 ± 1.0
	Tac 5	8.0 ± 1.1
	Tac 6	8.9 ± 1.0
	Tac 7	9.8 ± 1.3
SW	Tac 8	6.7 ± 1.0
	Tac 9	9.4 ± 1.3
Tacaná	Tac 10	5.3 ± 0.64
	Tac 11	0.7 ± 0.20
	Tac 12	7.0 ± 0.81
Ardillas	Tac 13	0.34 ± 0.10
	Tac 14	-
	Tac 15	0.17 ± 0.07
Andesitic	Tac 16	0.47 ± 0.11
	Tac 17	0.29 ± 0.09
	Tac 18	0.44 ± 0.11

Figure 6. Geological map of Tacaná Volcanic Complex. The red spots indicate the location of the samples collected for ^{36}Cl CRE dating.

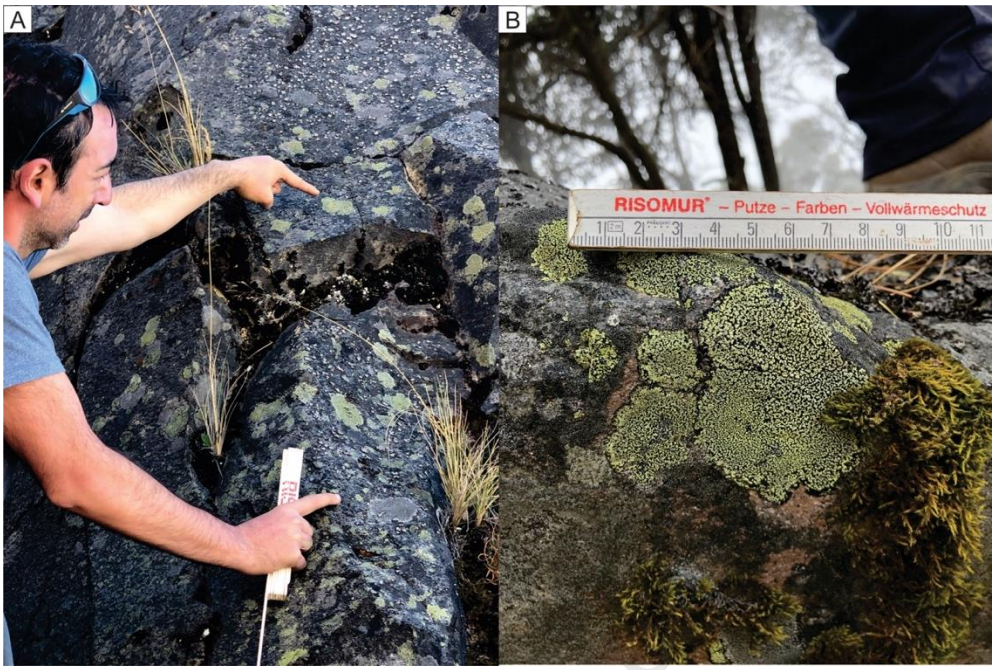


Figure 7. Detailed photographs of *Rhizocarpon geographicum*. A) A colony formed by several individuals whom oldest specimen is 390 years, growing on the surface of the "Andesitic lava"; B) The biggest specimen of *Rhizocarpon geographicum* found at the Ardillas dome yield a minimum age of 300 years.

5. Discussion

5.1. Interpretation of the ^{36}Cl CRE, lichenometry and dendrochronological ages

In this study, ^{36}Cl CRE dating was used to determine the age of four lava domes, one horseshoe-shaped crater and one lava from the summit and the upper part of TVC. Based on the geomorphology and field observations, the oldest rocks of the TVC summit seem to be the lavas cut by the collapse scar, followed by lavas that filled the horseshoe-shaped crater ending with extrusion of the summit domes (Figs. 2 and 6). The ^{36}Cl CRE ages obtained from the three summit lava domes are statistically indistinguishable considering their associated uncertainties and provide evidence of an important effusive episode at around 9 ka. These ages are in good agreement with the explosive Once de Abril eruption that occurred ca.10 ka (^{14}C age) and dispersed a succession of dense and dilute PDCs (Macías et al., 2015). Also at ca. 10 ka (Limón-Hernández, 2011), another debris avalanche, called Tuimanj, occurred towards the north associated with a smaller collapse on the northern part of the Tacaná scar crater (at Tuimanj hamlet). Hence, Once de Abril

570 eruption and Tuimanj debris avalanche were followed by a voluminous effusive cycle that
571 emplaced the three summit lava domes.

572 Based on the morphology and erosion of the Tacaná summit, it can be deduced that the first
573 dome extruded inside the horseshoe-shaped crater was the "East" dome (radio anthenna) at
574 9.3 ± 1.9 ka. It is quite likely that during its growing stage, parts of the dome collapse to the
575 west producing a N-S scar. This is a common feature in growing domes in which unstable
576 parts fail due to the action of the gravity (e.g. Colima volcano, Saucedo et al., 2004).
577 Afterwards, a new batch of andesitic magma emplaced to the west of this N-S scar erecting
578 first the "Northwest" (8.9 ± 0.9 ka) and shortly after the "Southwest" (8.6 ± 1.7 ka)
579 andesitic domes. The tree ages around the summit area range from 83 to 164 years, being in
580 good agreement with that of <100 years inferred from the thali of *Rhizocarpon*
581 *geographicum*. Obviously, these two ages are not related to the emplacement of the summit
582 domes ("East", "Northwest", and "Southwest"), but indicate growth recovery after the 1902
583 eruption of Santa Maria volcano that covered the summit of Tacaná with at least 15 cm of
584 ash. This eruption produced a tree-ring growth suppression event in the *Pinus hartwegii*
585 recorded from 1903 to 1908 (Carlón et al., 2020). Therefore, the ^{36}Cl CRE results document
586 that intense effusive activity filled the summit of Tacaná during the Early Holocene.

587 By contrast, the ^{36}Cl CRE ages of ca. 5-7 ka for the lava forming the southern edge of the
588 horseshoe-shaped crater are around 9 ka younger than the associated debris avalanche
589 deposit according to its ^{40}Ar/^{39}Ar age of 15 ± 5 ka (Macías et al., 2010). Further, they are
590 not consistent with the ^{36}Cl CRE ages of the summit domes (ca. 9 ka), which are
591 stratigraphically younger than the horseshoe-shaped crater and chemically
592 undistinguishable from the samples of the domes (Fig. 5b-g). We therefore infer an
593 underestimation of the ^{36}Cl CRE ages of the horseshoe-shaped crater and hypothesize that
594 gravitational processes affected the limit of the steep cliff of the horseshoe-shaped crater
595 from where the samples were collected. This implies that the sampled surfaces were
596 exposed several thousand years after the collapse event. Therefore, we assume that the ^{36}Cl
597 CRE ages should be considered as minimum ages of the volcanic collapse.

As the Ardillas lava dome is older than 760 ± 30 yr BP (Macías et al., 2018), we suspect that the ^{36}Cl CRE dates (0.3 ± 0.1 ka) underestimate the age of the emplacement of this dome. The sampled sites at this structure were to the right of the tensional fractures and very close to an unstable vertical cliff (Fig. 2 and supplement material) to the east sector of the dome. There is evidence of landslides associated probably with the stress regime enhanced by seismicity (Servicio Sismológico Nacional, UNAM; http://www.ssn.unam.mx) and heavy rainfalls with an annual precipitation between 4,500 and 5,000 mm (http://www.tapachula.gob.mx). Thus, we assume that we dated the approximate age of a landslide and not the age of the dome extrusion. Dendrochronology and lichenometry confirm the ^{36}Cl CRE dates with trees ranging between 117 and 164 years and lichen ages of 300 years, respectively. These results show that *in situ*-produced cosmogenic nuclide dating is useful to provide chronological constraints on active mass wasting processes in volcanic environments. Such a scenario further suggests that a monitoring studio (cameras, seismic stations) of these steep cliffs of the Ardillas dome might be necessary to alert downstream populations of future landslides.

A young ^{36}Cl CRE age (0.4 ± 0.1 ka) has also been obtained from the "Andesitic lava". Here, samples were collected from the west margin of the lava, which seems to be affected by a small landslide that exhibits a crater-like morphology opened to the west (Fig. 6 and supplement material; samples Tac 16-18). Chronological data from lichenometry (390 years) also support the ^{36}Cl CRE age, demonstrating a consistent young exposure of the sampled area. Given the observations of instability, we suggest that the ^{36}Cl CRE and lichenometry ages represent the age of a historical collapse likely associated with the phreatic explosion crater present at the base of the large NE-SW landslide that dispersed breccia and pyroclastic deposits atop the lava flow. In this sense, more research must be carried out to determine the exact age of the eruption not reported yet.

5.2. Refined Holocene volcanic history of TVC and hazards implications

After the ca.15 ka collapse of Tacaná that left a horseshoe-shaped crater, renewed activity ensued andesitic lavas (e.g. ca.12 ka Agua Zarca) that partially filled the collapse depression and crater. At around 10 ka, the largest explosive Holocene event of Tacaná

628 took place with the generation of PDCs that were dispersed radially around the volcano
629 affecting up to the base of the cone (Macías et al 2010). This eruption was produced during
630 open vent conditions (no domes involved atop), ejecting a low altitude eruptive column that
631 was called the Once de Abril ash flow sequence (Macías et al., 2015). At about the same
632 time, another collapse generated the Tuimanj debris avalanche to the north (Limón-
633 Hernández, 2011) that was smaller than the Agua Caliente debris avalanche. After these
634 volcanic events, Tacaná experienced effusive activity with the emplacement of the "East"
635 lava dome at 9.3 ± 1.9 ka, followed by the extrusion of the "Southwest" and "Northwest"
636 lava domes at 8.6 ± 1.7 ka and 8.9 ± 0.9 ka (Fig. 6) that filled the horseshoe-crater as we
637 know it today.
638
639 Then, explosive activity took place around the summit of the TVC with at least nine small
640 eruptions: (i) Papales ash flow deposit 1 (8683-8180 cal yr BP) (Macías et al., 2015); (ii)
641 the Chocab pumice flow with charcoal embedded at 7933-7595 cal yr BP (García-Palomo
642 et al., 2006); (iii) a pyroclastic sequence of flows and surges dated at 6998-6400 cal yr BP;
643 (iv) a pyroclastic surge sequence with an underlying paleosol dated at 2920-2715 cal yr BP,
644 (v) a scoria block and ash flow with charcoal dated at 924-748 cal yr BP; and (vi), the
645 phreatomagmatic eruption followed by a sub-Plinian column that dispersed a pumice-rich
646 fallout some 935-748 cal yr BP (Macías et al., 2018), forming an elongated crater lake of
647 80 x 60 m in diameter (Fig. 2). We also report a minimum ^{36}Cl CRE age of the "Andesitic
648 lava" of 0.4 ± 0.1 ka that was emitted somewhere close to the Southwest dome. This age is
649 supported by chronological data from lichenometry (390 years). The "Andesitic lava" was
650 disrupted by an elongated explosion crater (60 x 25 m) made of breccia and pyroclastic
651 deposits dispersed on the lava flow. Based on its different composition, it is likely that the
652 "Andesitic lava" was emitted before the "Northwest" and "Southwest" domes. The olivine-
653 bearing lava and the dome samples display negative trends in MgO, Fe_2O_3, CaO, and Al_2O_3
654 (Fig. 5b-g), suggesting their magmatic link and fractional crystallization of mafic phases at
655 depth (350 MPa; Mora et al., 2013). Besides, magma mixing between mafic melts and
656 andesitic magmas hosted in the reservoir can produce mafic enclaves (Coombs et al., 2003;
657 Mora et al., 2013); such mixing mechanism is commonly considered as a trigger of
658 volcanic eruptions (Manrique et al., 2020). Furthermore, the young ^{36}Cl CRE dates

659 determined for the Ardillas lava dome (0.2 ± 0.1 ka) and the "Andesitic lava" flow (0.4 ±
660 0.1 ka) testify the occurrence of active gravitational processes. These processes are related
661 to a NE-SW fissure along which occur tensional fractures, landslide scars, vents of
662 phreatomagmatic and phreatic explosions (e.g. 1986 explosion), hydrothermal fluids, and
663 fumaroles.

664 Three more historical explosive eruptions have been recognized on the slopes of Tacaná
665 volcano. One of them produced a yellow pyroclastic flow deposit dated at 536-157 cal yr
666 BP (Limón-Hernández, 2011). Another one produced an ash flow deposit called the Papales
667 ash flow dated at 496 - To Present cal yr BP (Macías et al., 2015), whereas a white
668 pyroclastic surge deposit was dated at 285 - To Present cal yr BP (Macias et al., 2015). The
669 last events at Tacaná were small explosions that took place during the last two centuries in
670 1855-1856 (Mercado and Rose, 1992; Carlón et al., 2020), 1949 (Müllerried 1951), and
671 1986 (De la Cruz-Reyna et al., 1989).

672 The presence of lava domes (ca. 9 ka) at the Tacaná summit (together with the lava
673 emplaced to the north) infilling the horseshoe-shaped crater suggests that after the ca.15 ka
674 sector collapse (Agua caliente debris avalanche), the activity shifted from explosive to
675 effusive eruptions, lasting for centuries or thousands of years. This is a common
676 phenomenon observed in many volcanoes after a sector collapse (e.g. Popocatépetl, Siebe
677 et al., 2017) probably related to degassing of magma. Furthermore, lava domes represent
678 the location of volcanic conduits from which magma was ejected to the surface. Thus, the
679 summit lava domes of Tacaná volcano emplaced during Early Holocene blocked the
680 volcanic conduit because no other craters are exposed at the summit today. Therefore, the
681 question arises where the vent responsible for the Late to Middle Holocene explosive
682 eruptions is located. A blockage of the conduit in the meantime could prevent the degassing
683 of the magma reservoir producing overpressure and eventually explosive eruptions when
684 the internal pressure reaches the rupture pressure of the surface. This could have produced
685 the nine dated explosive eruptions at the TVC (Macías et al., 2015). The magma
686 accumulated in the reservoir sought other paths to get to the surface as the set of NE-SW
687 fractures observed nowadays (Fig. 4) from which the phreatomagmatic explosion formed a
688 crater-lake around 0.76 ka (Macías et al., 2015), that was drained during the historic

689 phreatic explosion of 1949. The study of lava domes has important implications to specify
690 the behavior of eruption style (explosive-effusive) and the generation of block-and-ash
691 flows (i.e.: Colima volcano; Saucedo et al., 2002) that are one of the most dangerous
692 phenomena in explosive events (Vázquez et al., 2019). Explosive eruptions like those dated
693 at 5 and 2 ka (Macías et al., 2015) could be related to the gravitational collapse of the
694 external parts of summit domes and/or lava fronts (Saucedo et al., 2019).

695 We have recognized two NE-SW and two NW-SE scar collapses around the TVC summit.
696 These scar collapses have orientations in agreement with the present stress regime in the
697 area. Geometrically, this suggests that the location and evolution of the TVC could be
698 related to fractures with a N65° E to N75° E direction, which are in good agreement with
699 the results of García-Palomo et al. (2006), and could be associated with a large-scale
700 fracture with the same orientation (Fig. 4). Such stress regime and fault system is typical of
701 an active transtensive tectonic environment. Because no primary volcanic deposits are
702 associated with these events (i.e. debris avalanche deposits, or fallout and pyroclastic flow
703 deposits), they likely were produced by gravitational collapses only. The Tacaná summit
704 domes are highly viscous based on their acidic andesitic to dacitic compositions with
705 pronounced steep edges representing unstable parts prone to collapse. In addition, current
706 Google Earth images show active landslides taking place in the eastern portion of Ardillas
707 dome and the northeastern part of San Antonio volcano. This area is affected by the NE-
708 SW tension fractures displayed in figure 4, which past landslides dated in this study
709 ("Andesitic lava" and Ardillas dome) area associated with it. Therefore, this persistent
710 volcanic activity and mass waste processes highlight the need for a permanent monitoring
711 system of the complex, which would be essential to predict future geologic hazards and
712 mitigate the associated risks for the nearby populations.

713 A better constraint of the eruptive chronology of the Holocene activity of the TVC has been
714 complemented with our results highlighting an intense effusive volcanic and landslide
715 activity during the Holocene. This Holocene volcanic activity of the TVC is similar to other
716 volcanes in Mexico as Colima and Popocatépetl. Colima volcano (the most active volcano
717 in Mexico) has experienced at least nine explosive eruptions intercalated with dome-
718 forming events (Macías and Arce, 2019), and several small-magnitude eruptions (1991,

2000, 2002, 2006, 2015) (Rodríguez-Elizarrarás et al., 1991; Saucedo et al., 2005, 2010; Mora et al., 2004; Capra et al., 2016). Popocatépelt volcano has recorded 12 explosive eruptions during the Holocene (Macías and Arce, 2019), involving three large magnitude Plinian eruptions (Siebe et al., 1995; Siebe and Macías, 2006). Therefore, the TVC stands among the most active (hazardous) volcanoes in Mexico during the Holocene. In terms of risk, however, the TVC is the second most dangerous volcano just after Popocatépetl, because a future eruption would threaten more than around 300,000 people, including the city of Tapachula. A Plinian eruption would disrupt life in Central America affecting main cities of Belize, Guatemala, El Salvador, Honduras, and Mexico (Vázquez et al., 2019).

6. Conclusions

^{36}Cl CRE dating, dendrochronology and lichenometry were combined to determine the unknown ages of lava domes, a steep cliff of the late Pleistocene horseshoe-shaped crater, and one lava from Tacaná volcano. The summit lava domes ("East", "Northwest" and "Southwest") are dated consistently at 9.3 ± 1.9 ka; 8.9 ± 0.9 ka; 8.6 ± 1.7 ka, providing evidence of a voluminous effusive activity around 9 ka that followed a major explosive eruption of Tacaná (Once de Abril ash flow sequence).

Furthermore, ^{36}Cl CRE ages of the cliff of the horseshoe-shaped crater of ca. 5-7 ka most likely correspond to gravitiational rock fall events rather than to the collapse event of the crater, which is expected to predate the summit domes according to the volcanic stratigraphy. Strikingly, the combination of ^{36}Cl CRE ages, lichenometry and dendrochronology in the "Andesitic lava" and Ardillas dome resulted also useful to detect active processes associated with NE-SW landslide scars, explosion craters, phreatic vents, fumarole activity, and tensional fractures all of which are perpendicular to the NW-SE minimum stress regime ($\sigma 3$) in the area. Therefore, we conclude that Tacaná is one of the most active volcanoes in Mexico, probably the third just after the Colima and Popocatépetl volcanoes. This scenario implies the need for a significant effort to mitigate volcanic hazards and associated risks (i. e. volcanic collapses) that can affect the nearby populations.

Acknowledgements

This research was supported by Consejo Nacional de Ciencia y Tecnología (CONACyT) projects A1-S-21156 to J. Alcalá Reygosa and PN522 to J.L. Macías. Dirección de Asuntos del Personal Académico (DGAPA-PAPIIT) IN112720 to J.L. Macías, and IN101620 to J.L. Arce. The ^{36}Cl measurements were performed at the ASTER AMS national facility (CEREGE, Aix en Provence) which is supported by the INSU/CNRS, the ANR through the "Projets thématiques d'excellence" program for the "Equipements d'excellence" ASTER-CEREGE action and IRD. We are also grateful to Irma Fabiola Mendiola López and Omar López Arevalo (Instituto de Geofísica Unidad Morelia; Universidad Nacional Autónoma de México) whom helped in the physical treatment of the ^{36}Cl samples. We are indebted with J.I. Lara, A. Lugo, M. Mendoza, G. Sosa for sharing field campaings with us at the volcano. We are grateful for the constructive comments by Naki Akcar and Venera R. May whom greatly improved the manuscript.

References

Alcalá-Reygosa, J., Palacios, D., Schimmelpfennig, I., Vázquez-Selem, L., García-Sancho, L., Franco-Ramos, O., Villanueva, J., Zamorano, J. J., Aster Team (Aumaitre, G., Bourlès, D., Keddadouche, K.) 2018a. Dating late Holocene lava flows in Pico de Orizaba (Mexico) by means of in situ-produced cosmogenic ^{36}Cl, lichenometry and dendrochronology. Quaternary Geochronology 47, 93-106. https://doi.org/10.1016/j.quageo.2018.05.011.

Alcalá-Reygosa, J., Arce, J. L., Schimmelpfennig, I., Salinas, E. M., Rodríguez, M. C., Léanni, L., Aster Team (Aumaitre, G., Bourlès, D., Keddadouche, K.) 2018b. Revisiting the age of the Jumento volcano, Chichinautzin Volcanic Field (Central Mexico), using in situ-produced cosmogenic 10Be. Journal of Volcanology and Geothermal Research 366, 112-119. https://doi.org/10.1016/j.jvolgeores.2018.10.005.

Arce, J.L., Macías, J.L., Vázquez-Selem, L. 2003. The 10.5 ka Plinian eruption of Nevado de Toluca, Mexico: stratigraphy and hazard implications. Geological Society of America Bulletin 115, 230-248.

Arce, J.L., Macías, J.L., Gardner, J.E., Rangel, E., 2012. Reconstruction of the Sibinal Pumice, an andesitic Plinian eruption at Tacaná Volcanic Complex, Mexico-Guatemala. Journal of Volcanology and Geothermal Research 217-218, 39-55. https://doi.org/10.1016/j.jvolgeores.2011.12.013.

779 Arce, J.L.**,** Walker, J., Keppie, J. D., 2015. Petrology and geochemistry of El Chichón and
780 Tacaná: two active, yet contrasting Mexican volcanoes. In: Active Volcanoes of Chiapas
781 (Mexico): El Chichón and Tacaná. Edited by T. Scolamacchia and J.L. Macías. Springer-
782 Verlag, 25-43 p. https://doi:10.1007/978-3-642-25890-9_2.

783 Arnold, M., Aumaître, G., Bourlès, D. L., Keddadouche, K., Braucher, R., Finkel, R. C.,
784 Nottoli, E., Benedetti, L., Merchel, S. 2013. The French accelerator mass spectrometry
785 facility ASTER after 4 years: status and recent developments on ^{36}Cl and ^{129}I. Nuclear
786 Instruments and Methods in Physical Research 294, 24-28.
787 https://doi.org/10.1016/j.nimb.2012.01.049.

788 Capra, L., Macías J.L., Cortés, A., Davila, N., Saucedo, R., Osorio-Ocampo, S., Arce, J.L.,
789 Gavilanes-Ruíz, J.C., Corona-Chávez, P., García-Sánchez, L., Sosa-Ceballos, G., Vázquez,
790 R. 2016. Preliminary report on the July 10-11, 2015 eruption at Volcán de Colima:
791 Pyroclastic density currents with exceptional runouts and volumes. Journal of
792 Volcanolology and Geothermal Research 310, 39-49.
793 https://doi.org/10.1016/j.jvolgeores.2015.11.022.
794
795 Carlon, T., Macías, J.L., Mendoza, M., and Villanueva, J. 2020. Evidence of volcanic
796 activity in the growth rings of trees in the Tacaná Volcano, Mexico-Guatemal. Journal of
797 Canadian Forest 50: 65-72. http://doi.org/10.1139/cjfr-2019-0214.
798
799 Coombs, M. L., Eichelberger, J. C., Rutherford, M. J. 2003. Experimental and textural
800 constraints on mafic enclave formation in volcanic rocks. Journal of Volcanology and
801 Geothermal Research 119, 125-144. https://doi.org/10.1016/S0377-0273(02)00309-8.
802
803 De la Cruz-Reyna, S., Armienta, M.A., Zamora, V., Juárez, F. 1989. Chemical changes in
804 spring waters at Tacaná Volcano, Chiapas, México. Journal of Volcanolology and
805 Geothermal Research 38, 345-353. https://doi.org/10.1016/0377-0273(89)90047-4.

806 Dunai, T.J., 2010. Cosmogenic nuclides. Principles, Concepts and Applications in the
807 Earth Surface Sciences. Cambridge University Press, pp. 198.

808 Espíndola, J. M., Medina, F. M., and De los Ríos, M., 1989. A C-14 age determination in
809 the Tacaná volcano (Chiapas, Mexico). Geofisica Internacional 28, 123-128.

810 Fink, D., Vogt, S., Hotchkis, M. 2000. Cross-sections for ^{36}Cl from Ti at Ep =35–150
811 MeV: applications to *in-situ* exposure dating. Nuclear Instruments and Methods in Physical
812 Research Section B Beam Interaction Mater and Atoms 172, 861-866.
813 https://doi.org/10.1016/S0168-583X(00)00200-7.
814

Journal Pre-proof

García-Palomo, A., Macías, J.L., Arce, J.L., Mora, J.C., Hughes, S., Saucedo, R., Espíndola, J.M., Escobar, R., Layer, P. 2006. Geological evolution of the Tacaná Volcanic Complex, México-Guatemala. In: Rose WI, Bluth GJS, Carr MJ, Ewert JW, Patino LC, Vallance JW (eds) Natural Hazards in Central America. Boulder, Colorado. Geological Society of America, Special Paper 412, 39-57. https://doi.org/10.1130/2006.2412(03).

Garduño, V.H., Macías, J.L., Molina, R. 2015. Geodynamic setting and pre-volcanic geology of active volcanism in Chiapas. In: Active Volcanoes of Chiapas (México): El Chichón and Tacaná. Edited by T. Scolamacchia and J.L. Macías. Springer Verlag, 1-24. DOI 10.1007/978-3-642-25890-9_1.

Jomelli, V., Lane, T., Favier, V., Masson-Delmotte, V., Swingedouw, D., Rinterknecht, V., Schimmelpfennig, I., Brunstein, D., Verfaillie, D., Adamson, K., Leanni, L., Mokadem, F., Aumaitre, G., Bourles, D.L., Keddadouche, K. 2016. Paradoxical cold conditions during the medieval climate anomaly in the Western Arctic. Scientific Reports 6, 32984. http://dx.doi.org/10.1038/srep32984.

Limón-Hernández, C. G. 2011. Estratigrafía y morfología de los flujos de lava y depósitos asociados a la actividad efusiva del volcán Tacaná, México-Guatemala. Master thesis, Posgrado en Ciencias de la Tierra UNAM, México, 125 p.

Macías J. L, Espíndola J. M, García-Palomo A, Scott K. M, Hughes S, Mora J. C 2000. Late Holocene Peléan style eruption at Tacaná Volcano, Mexico-Guatemala: Past, present, and future hazards. Bulleting Geological Society of America 112, 1234-1249.
https://doi.org/10.1130/00167606(2000)112<1234:LHPEAT>2.0.CO;2

Macías, J.L., Arce, J.L., García-Palomo, A., Mora, J.C., Layer, P.W., Espíndola, J.M. 2010. Late-Pleistocene flank collapse triggered by dome growth at Tacaná Volcano, México-Guatemala, and its relationship to the regional stress regime. Bulletin of Volcanology 72, 33-53.

Macías, J.L., Arce, J.L., Layer, P.W., Saucedo, R., Mora, J.C. 2015. Eruptive history of the Tacaná Volcanic Complex. In: Scholamacchia T, Macías JL (Eds.) Active Volcanoes of Chiapas (Mexico) El Chichón and Tacaná, Active Volcanoes of the world, Springer Verlag pp. 115-138.

Macías, J.L., Arce, J.L., Capra, L., Saucedo, R., Sánchez-Núñez, J.M. 2018. Late Formative flooding of Izapa after an eruption of Tacaná volcano. Ancient Mesoamerica 29:361-371.

Macías, J. L., Arce, J. L. 2019. Volcanic Activity in Mexico During the Holocene. In The Holocene and Anthropocene Environmental History of Mexico (pp. 129-170). Springer, Cham. https://doi.org/10.1007/978-3-030-31719-5_8.

Manrique, N., Samaniego, P., Médard, E., Schiavi, F., Mariño, J., Liorzou, C. 2020. Pre-eruptive magmatic processes associated with the historical (218 ± 14 aBP) explosive eruption of Tutupaca volcano (southern Peru). Bulletin of Volcanology, 82:6, https://doi.org/10.1007/s00445-019-1335-4.

Marrero, S. M., Phillips, F. M., Caffee, M. W., Gosse, J. C., 2016. CRONUS-Earth cosmogenic ^{36}Cl calibration. Quaternary Geochronology 31, 199-219. https://doi.org/10.1016/j.quageo.2015.10.002.

Martíni, M., Capaccioni, B., Giannini, L., 1987. Ripresa dell'attivita sismica e fumarolica al Vulcano di Tacaná (Chiapas, Messico) dopo un quarantennio di quiescenza. Estrato da Bollettino del Grupo Nazionale per la Vulcanología, 467-470.

Mercado, R., Rose, W.I. 1992. Reconocimiento geológico y evaluación preliminar de peligrosidad del Volcán Tacaná, Guatemala/México. Geofísica Internacional 31(3): 205-237.

Merchel, S., Bremser, W., Alfimov, V., Arnold, M., Aumaître, G., Benedetti, L., Bourles, D.L., Caffee, M., Fifield, L.K., Finkel, R.C., Freeman, S.P.H.T., Martschini, M., Matsushi, Y., Rood, D.H., Sasa, K., Steier, P., Takahashi, T., Tamari, M., Tims, S.G., Tosaki, Y., Wilcken, K.M., Xu, S., 2011. Ultra-trace analysis of 36Cl by accelerator mass spectrometry: an interlaboratory study. Anal. Bio- anal. Chem. https://doi.org/10.1007/s00216-011-4979-2.

Mora, J.C., Macías, J.L., García-Palomo, A., Espíndola, J.M., Manetti, P., and Vaselli, O. 2004. Petrology and geochemistry of the Tacaná Volcanic Complex, Mexico-Guatemala: Evidence for the last 40 000 yr of activity. Geofísica Internacional 43, 331-359.

Mora, J. C., Gardner, J. E., Macías, J. L., Meriggi, L. 2013. Magmatic controls on eruption dynamics of the 1950 yr B.P. eruption of San Antonio Volcano, Tacaná Volcanic Complex, Mexico–Guatemala. Journal of Volcanology and Geothermal Research 262, 134-152. https://doi.org/10.1016/j.jvolgeores.2013.06.002.

Müllerried, F.K.G., 1951. La reciente actividad del Volcán Tacaná, Estado de Chiapas, a fines de 1949 y principios de 1950. Informe del Instituto de Geología, UNAM, 28p.

N.O.A.A, 1976. U.S. Standard Atmosphere. US Gov. Print. Off.

887 Palacios, L., García-Sancho, Zamorano, J.J., Andrés, N., Pintado, A., 2012. The
888 deglaciation of Iztaccíhuatl volcano (Mexico) from the Little Ice Age maximum to the
889 present, determined by photogrametry and lichenometry. Geophysical Research Abstracts
890 14, EGU2012–3755 2012.

891 Rodriguez-Elizarrarás, S., Siebe, C., Komorowski, J. C., Espíndola, J. M., Saucedo, R.
892 1991. Field observations of pristine block and ash flow deposits emplaced April 16-17
893 1991 at Volcán de Colima, Mexico. Journal of Volcanology and Geothermal Research 48
894 (3-4), 399-412. https://doi.org/10.1016/0377-0273(91)90054-4.

895 Rouwet, D., Taran, Y., Inguaggiato, S., Varley, N. 2004. Hydrothermal activity at Tacaná
896 volcano, Mexico–Guatemala. In: Wanty R, Seal R II (eds) WRI-11. Taylor and Francis
897 Group, London, 173–176.

898 Rouwet, D., Inguaggiato, S., Taran, Y., Varley, N., Santiago, J.A., 2009. Chemical and
899 isotopic compositions of thermal springs, fumaroles and bubbling gases at Tacaná Volcano
900 (Mexico-Guatemala): implications for volcanic surveillance. Bulletin of Volcanolology 71,
901 319-335.

902 Saucedo, R., Macías, J.L., Bursik, M., Mora, J.C., Gavilanes, J.C., Cortes, A. 2002.
903 Emplacement of pyroclastic flows during the 1998-1999 eruption of Volcán de Colima,
904 Mexico. Journal of Volcanology and Geothermal Research 117 (1-2), 129-153.
905 https://doi.org/10.1016/S0377-0273(02)00241-X.

906 Saucedo, R., Macías, J.L., and Bursik, M.I., 2004. Merapi-type pyroclastic flows produced
907 during the 1991 eruption of Colima Volcano: stratigraphy, sedimentology and emplacement
908 mechanisms. Bulletin of Volcanology 66, 291-306.

909 Saucedo, R., Macías, J.L., Sheridan, M.F., Bursik, M.I., Komorowski, J.C. 2005. Modeling
910 of pyroclastic flows of Colima Volcano, Mexico: Implications for hazard
911 assessment. Journal of Volcanology and Geothermal Research 139, 103-115.
912 https://doi.org/10.1016/j.jvolgeores.2004.06.019.
913
914 Saucedo, R., Gavilanes-Ruiz, J.C., Macías, J.L., Arce, J.L., Komorowski, J.C., Gardner, J.,
915 Valdez-Moreno, G., (2010). Eyewitness, stratigraphy, chemistry, and eruptive dynamics of
916 the 1913 Plinian eruption of Volcán de Colima, México. Journal of Volcanology and
917 Geothermal Research, 191: 149-166. https://doi.org/10.1016/j.jvolgeores.2010.01.011.

918 Saucedo, R.1, Macías, J.L., Gavilanes-Ruiz, J.C., Bursik, M.I., and Vargas-Gutiérrez, V.,
919 2019. Pyroclastic density currents at Volcán de Colima. N. Varley et al. (eds.), Volcán de

Colima, Active Volcanoes of the World, https://doi.org/10.1007/978-3-642-25911-1_4, Chapter 12, 111-140 p.

Schimmelpfennig, I., Benedetti, L., Finkel, R., Pik, R., Blard, P. H., Bourle, D., Burnard, P., Williams, A. 2009. Sources of in-situ ^{36}Cl in basaltic rocks. Implications for calibration of production rates. Quaternary Geochronology 4, 441-461. https://doi.org/10.1016/j.quageo.2009.06.003.

Schimmelpfennig, I., Benedetti, L., Garreta, V., Pik, R., Blard, P. H., Burnard, P., Bourlès, D., Finkel, R., Ammon, K., Dunai, T. 2011. Calibration of cosmogenic ^{36}Cl production rates from Ca and K spallation in lava flows from Mt. Etna (38ºN, Italy) and Payun Matru (36ºS, Argentina). Geochimica et Cosmochimica Acta 75, 2611-2632. **10.1016/j.gca.2011.02.013.**

Schimmelpfennig I, Schaefer J, Putnam A, Koffman T, Benedetti L, Ivy- Ochs S, ASTER Team, Schlüchter C. 2014. ^{36}Cl production rate from K-spallation in the European Alps (Chironico landslide, Switzerland). Journal of Quaternary Science 29, 407-413. https://doi.org/10.1002/jqs.2720.

Siebe, C.G., Macías, J.L., Abrams, M., Elizarraras, R.S., Castro, R., Delgado, H. 1995. Quaternary Explosive Volcanism and Pyroclastic Deposits in East-Central Mexico: Implications for Future Hazards. In: Chacko, J.J., and Whitney, J.A., (Eds.), Guidebook of Geological Excursions for the 1995 Annual Meeting of the Geological Society of America, New Orleans, Book 1, p. 1-48.

Siebe, C., Macías, J.L. 2006. Volcanic hazards in the Mexico City metropolitan area from eruptions at Popocatepetl, Nevado de Toluca, and Jocotitlán stratovolcanoes and monogenetic scoria cones in the Sierra de Chichinautzin Volcanic Field. *in* Siebe, C., Macías, J.L., and Aguirre-Díaz, G.J., eds., Neogene-Quaternary continental margin volcanism: A perspective from Mexico. Geological Society of America. Special Paper 402, p. 237–252. doi: 10.1130/2006.2402(05).

Siebe, C., Salinas, S., Arana-Salinas, L., Macías, J.L., Gardner, J., and Bonasia, R., 2017. The ~23,500 yr ^{14}C BP White Pumice Plinian eruption and associated debris avalanche and Tochimilco lava flow of Popocatépetl volcano, México. Journal of Volcanology and Geothermal Research 333–334, 66-95. https://doi.org/10.1016/j.jvolgeores.2017.01.011.

Stone, J., 2000. Air pressure and cosmogenic isotope production. Journal of Geophysical Research 105, 23,753-23,759. https://doi.org/10.1029/2000JB900181.

953 Stone, J.O., Fifield, K., Vasconcelos, P., 2005. Terrestrial chlorine-36 production from
954 spallation of iron. In: 10th International Conference on Accelerator Mass Spectrometry,
955 Berkeley, USA.

956 Stokes, M.A., Smiley, T.L. 1996. An introduction to tree-ring dating. The University of
957 Arizona Press, Tucson, Arizona.
958
959 Vázquez-Selem, L., Heine, K., 2011. Late quaternary glaciation in Mexico. In: Ehlers, J.,
960 Gibbard, P.L., Hughes, P.D. (Eds.), Quaternary Glaciations - Extent and Chronology. A
961 Closer Look. Elsevier, Amsterdam, pp. 849–861. http://doi.org/10.1016/B978-0- 444-
962 53447-7.00061-1.
963
964 Vázquez, R., Bonasia, R., Folch, A., Arce, J.L., Macías, J.L. 2019. Tephra fallout hazard
965 assessment at Tacaná volcano (Mexico). Journal of South American Earth Sciences 91,
966 253-259. https://doi.org/10.1016/j.jsames.2019.02.013.

967 Vermeesch, P., 2007. CosmoCalc: an excel add-in for cosmogenic nuclide calculations. G-
968 cubed 8, 1525-2027.

969 Ward, G. K., Wilson, S. R. 1978. Procedures for comparing and combining radiocarbon age
970 determinations: a critique. Archaeometry 20 (1), 19-31. https://doi.org/10.1111/j.1475-
971 4754.1978.tb00208.x.
972
973 Williams, S. N., Self, S., 1983. The October 1902 Plinian eruption of Santa Maria volcano,
974 Guatemala. Journal of Volcanology and Geothermal Research 16, 33-56.
975 https://doi.org/10.1016/0377-0273(83)90083-5.

976

977

978

979

980

981

982

Journal Pre-proof

983

984

985

986

987

988 **SUPPLEMENTS**

Journal Pre-proof

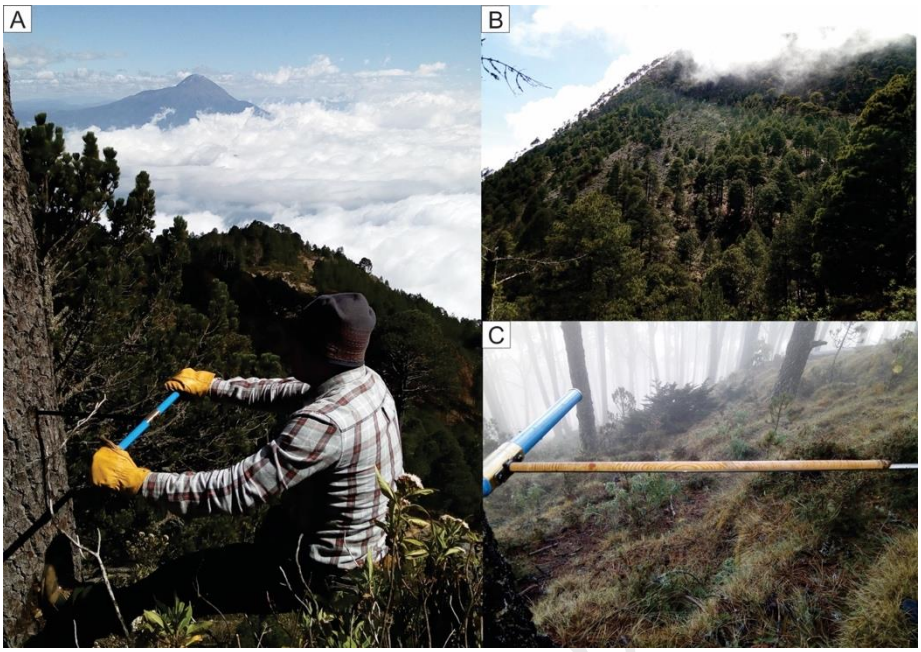


Detailed photographs of the samples collected for ^{36}Cl CRE dating from the summit lava domes of Tacaná volcano.



995

996 Detailed photographs of the samples collected for ^{36}Cl CRE dating from the cliff collapse scar, the
997 Ardillas dome and the "Andesitic lava" from Tacaná Volcanic Complex.
998



Detailed photographs of the samples collected for dendrochronology. A) Sampling a specimen of *Pinus hartwegii* Lindl using a Häglof borer perpendicular to the stem and at breast height; B) Forest of *Pinus hartwegii* Lindl that grows on Ardillas dome; C) Detailed of the sample from a specimen of *Pinus hartwegii* Lindl. The ages range between 117 to 164 years.

Journal Pre-proof

Journal Pre-proof

Declaration of interests

√ The authors declare that they have no known competing financial interests or personal relationships that could have appeared to influence the work reported in this paper.

☐The authors declare the following financial interests/personal relationships which may be considered as potential competing interests:

Journal Pre-proof